TÉCNICO LISBOA

Comparative study of the toxicity of synthetic nanoparticles to yeast *Saccharomyces cerevisiae*

Daniela de Almeida Correia

Thesis to obtain the Master of Science Degree in

Biotechnology

Supervisors: Prof. Dr. Maria Teresa Ferreira Marques Pinheiro

Prof. Dr. Isabel Maria de Sá-Correia Leite de Almeida

Examination Committee:

Chairperson: Prof. Dr. Arsénio do Carmo Sales Mendes Fialho

Supervisor: Prof. Dr. Maria Teresa Ferreira Marques Pinheiro

Members of the Committee: Prof. Dr. Ana Cristina Anjinho Madeira Viegas

December 2015

Acknowledgments

Firstly, I would like to thank to my advisor, Dr. Teresa Pinheiro, for the opportunity to develop this work at Centro Tecnológico e Nuclear (ITN), where part of this work was carried out. I am most thankful for her guidance, as well as for her prompt availability and willingness to support me during the development of this thesis. I would like to thank my co-advisor Prof. Isabel Sá-Correia for her helpful comments and suggestions and for giving me the opportunity to join of the Institute for Biotechnology and Bioengineering (IBB) where part of this work was developed.

I would like to thank all of and IBB and ITN members that helped me in any doubt that I had along the way, especially to Claudia Godinho, for all the time that she spent helping me in the lab.

I also would like to acknowledge my friends and family for their unconditional support and encouragement.

This work was financed by national funds through FCT - Foundation for Science and Technology, under the project UID/BIO/04565/2013

Resumo

O aumento da produção de nanopartículas de óxido de cobre (CuO-NPs) e suas múltiplas aplicações, deste os têxteis à eletrónica, levanta questões sobre os potenciais riscos destas NPs tanto ambientais como na saúde humana. No entanto, continua a faltar conhecimento cientifico sobre quais os mecanismos e modos de ação destas nanopartículas. Assim sendo, é crucial investir no conhecimento científico e no desenvolvimento de modelos e métodos de avaliação eficientes. O principal objetivo desta tese foi avaliar a toxicidade de CuO-NPs usando levedura *Saccharomyces cerevisiae* como modelo.

Tanto a estirpe *Saccharomyces cerevisiae* BY4741 (tipo selvagem) como a estipe mutante de eliminação simples BY4741_*Δcup2* (*cup2Δ*), associado a mecanismos de destoxificação de cobre, foram expostas a CuO-NPs, tendo como referência células expostas ao ião Cu^{2+} ($CuSO_4$). As características físicas e aglomeração de CuO-NPs, durante o decurso das experiências, foram examinadas com a técnica DLS (Dynamic Light Scattering). A curva de crescimento e a análise de unidades formadoras de colónias (CFU) das culturas expostas a CuO-NPs mostrou que ambas as estirpes apresentam susceptibilidade a CuO-NPs, sendo a estirpe selvagem mais vulnerável a CuO-NPs do que a concentrações equivalentes de $CuSO_4$. A capacidade das CuO-NPs induzir oxidação de proteínas foi confirmada através da determinação dos grupos tiol da proteína livres, por meio de imunoensaio. Técnicas de microscopia nuclear, baseadas em feixes de protões focados com dimensões micrométricas, com energias da ordem dos MeV, permitiram obter imagens da distribuição de Cu e a sua quantificação, em células individualizadas de *S. cerevisiae*. Verifica-se que ambas as estirpes apresentam maior concentração de Cu quando expostas a CuO-NPs relativamente a $CuSO_4$. A análise do perfil de Cu em profundidade, em células de S. cerevisiae selvagem e mutante utilizando a técnica de RBS (Rutherford Backscattering Spectrometry) permitiu concluir que o Cu derivado de CuO-NPs se acumula no interior das células.

Este trabalho preliminar destacou o potencial do uso de *S. cerevisiae* como modelo para o estudo da toxicidade de nanopartículas e a adequação das metodologias desenvolvidas para avaliação da bioacumulação de CuO-NPs.

Palavras-chave: Nanopartículas de óxido de cobre (CuO-NPs), *Saccharomyces cerevisiae*; resposta da levedura ao cobre, *cup2Δ*, Microscopia Nuclear

Abstract

The increasing production of copper oxide nanoparticles (CuO-NPs) and their multiple applications from textiles to electronics has led to major concerns regarding the potential hazards for the environment and for human health. However, conclusive scientific knowledge is still lacking for mechanisms and modes of action. The major objective of this Thesis was to evaluate the toxicity of CuO-NPs by using the yeast *Saccharomyces cerevisiae* as an experimental model.

Both parental strain *Saccharomyces cerevisiae* BY4741 and the mutant BY4741_*Δcup2* (*cup2Δ*), deleted for CUP2 gene associated to copper detoxification mechanisms, were exposed to CuO-NPs, having as reference cells exposed to the ionic form Cu^{2+} ($CuSO_4$). The physical characteristics and agglomeration of CuO-NPs during the course of the experiments were examined with Dynamic Light Scattering. The alterations of the growth curves based on the culture optic density and colony-forming units (CFU) analyses following exposure to CuO-NPs. Results showed that both strains were susceptible to CuO-NPs, being the wild-type strain more vulnerable to CuO-NPs than to equivalent concentrations of $CuSO_4$. The level of protein oxidation in *S. cerevisiae* stressed cells was studied based on the determination of protein free thiol groups. Results indicate that CuO-NPs induce protein oxidative damage. Nuclear microscopy techniques based on MeV proton beams focused to micrometre dimensions, assisted on the imaging of Cu distribution and quantification in whole individualized *S. cerevisiae* cells. The results showed higher Cu content in both wild-type and *cup2Δ* cells exposed to CuO-NPs than cultures exposed to $CuSO_4$. In addition, using the depth resolving capabilities of Rutherford Backscattering Spectrometry the Cu accumulation inside wild-type and mutant cells was confirmed.

This preliminary study highlighted the potential of *S. cerevisiae* as a model to study nanoparticles toxicity and the adequacy of the methodologies developed.

Keywords: Copper nanoparticles (CuO-NPs), *Saccharomyces cerevisiae*; copper tolerance, cup2, Nuclear Microscopy.

Content

List of Figures

List of Tables

List of Abbreviations

CFU	Colony-forming units
CuO-NPs	Copper oxide nanoparticles
cup2Δ	*Saccharomyces cerevisiae* BY4741_*Δcup2*
DLS	Dynamic Light Scattering
EUROSCARF	European *Saccharomyces cerevisiae* archive for functional analysis
MPB	Maleimide-PEG2-biotin
NPs	Nanoparticles
OD_{600nm}	Optical density at 600nm
PIXE	Particle Induced X-Ray Emission
RBS	Rutherford Backscattering Spectrometry
ROS	Reactive Oxygen Species
S. cerevisiae	*Saccharomyces cerevisiae*
STIM	Scanning Transmission Ion Microscopy
$t_{analysis}$	Acquisition time in Dynamic Light Scattering measurements
t_{eq}	Equilibration time in Dynamic Light Scattering measurements
TEM	Transmission Electron Microscopy

1 Motivations and thesis outline

Nowadays the exponential production of nanomaterials specially the increase of manufactured nanoparticles (NPs) on quotidian uses as well as in industrial and scientific applications[1–4] has lead to an increase in the concern about their short- and long-term toxicological effects in the environment, 'non-target' organisms and human health. Due to their possible accumulation [5], after release in the waste streams and further into the environment [3,6].

Physico-chemical properties of NPs including size, shape, surface charge and surface chemistry have been identified as strongly modulating the cellular uptake efficiency[7]. The foundation behind NPs cellular effects relate to increased reactivity resulting from their small size and the large number of surface atoms compared to their bulk counterparts. NPs transformations may modify their ability to translocate cell membranes, enhance electron transfer, bind of molecular species and interfere with the cell enzymatic machinery, which in turn influence the cell stability. However, how different NPs interact with cells and modulate their response are challenging issues, which require the development of efficient models and screening methods.

Like others NPs the CuO-NPs had been spreading through different fields of applications from electronics to cosmetics[3]. However the potential DNA damage caused by CuO-NPs, as well as its contribution to the development of diseases like cancer, arteriosclerosis and arthritis[8], turns these CuO-NPs into a relevant object of study, for better understanding of the real harmful potential of these NPs.

The used of *S. cerevisiae* as a biological model for the toxicological evaluation of NPs had increase due to several advantages like the similarity with higher-level organisms[2,9], the availability of systematic genome-wide mutant collections of yeast[9], the availability of genome-wide approaches to examine the global response to numerous environmental conditions[10,11] and the short generation time together with the easy and low cost of its cultivation in the laboratory[2]. Copper, even being an essential micro-nutrient in yeast, it is known to be toxic at high concentrations, since it can generate reactive oxygen species (ROS) that can oxidize nucleic acids, proteins and lipids[6,12–14]. Although the mechanisms of copper tolerance in yeast are well studied as far as ionic Cu forms are concerned (i.e., Cu^{+} and Cu^{2+}) and several single deletion mutants in genes associated with copper uptake and detoxification mechanisms are available, the mechanisms of toxicity of CuO-NPs are still largely unknown.

The major objective of this Master Thesis was to take a step forward in the evaluation of the toxicity of copper oxide NPs (CuO-NPs) by using the yeast *Saccharomyces cerevisiae* as an experimenal model.

Therefore the parental *Saccharomyces cerevisiae* strain BY4741 (MATa, his3Δ1, leu2Δ0, met15Δ0, ura3Δ0) and the derived single deletion mutant BY4741_*Δcup2*, which associates with Cu detoxification mechanisms conferring altered tolerance to Cu, were exposed to different

concentrations of CuO-NPs, having as reference cells exposed to the ionic form Cu^{2+} counterpart ($CuSO_4$), and non-exposed cells as controls.

To achieve this objective multiple approaches were used. Biological assays were used to assess cell growth and measure protein oxidative damage. The growth curves and the colony-forming units (CFU) were performed for cultures exposed to CuO-NPs to assess yeast strains susceptibility. The level of protein oxidation was studied, through the determination of protein free thiol groups to inspect whether the mechanisms of action of CuO-NPs are similar to the ionic Cu forms. Advanced nuclear microscopy techniques to image Cu distribution in whole yeast cells were used by us as an alternative to a more conventional approach for the imaging of the sub-cellular structure, like TEM, delivering images of elemental distributions as well as elemental quantification in cells. This technique provides a relatively good sub-micron lateral resolution images of the morphology of a tissue or cell and the corresponding elemental distributions in real-time, displaying sample features that cannot promptly be imaged by other techniques[15–17]. Elemental quantification has presented outstanding analytical sensitivity and quantitative precision (1–10 µg/g on a dry weight basis), especially for transition elements which are the essential trace elements in biological sistems[17]. By exploring the unique capabilities of Rutherford Backscattering Spectrometry technique the Cu depth profiles (reaching depth resolutions <100nm), can be established in a single cell.

All the experiments will take into account the physical characterization of the NPs. To better assess the potential toxicity of NPs in an *in vitro* toxicological assay, the physical characteristics of CuO-NPs and their agglomeration during the course of the experiments were studied by Dynamic Light Scattering. The study of NPs dispersion/agglomeration is essential since highly agglomerated NPs may have less toxicity compared to well-dispersed NPs[18].

It is expected to assess the viability of yeast strains when exposed to CuO-NPs and to estimate the consequences of such exposure on known mechanisms of Cu detoxification. Also it is expected to visualize Cu distribution in whole cells and determine the cell depth Cu profiles to confirm CuO-NPs internalization by cells.

2 Introduction

2.1 Applications of nanomaterials

Currently, the nanotechnology field is growing exponentially and nanomaterials are being incorporated into all aspects of life. Nanoindustry is one of the fastest growing industries in the history of mankind and has been referred to as the next industrial revolution[1–3]. The first national nanotechnology program—the National Nanotechnology Initiative—was launched in USA in 2000. In 2010, the worldwide annual funding (public as well as private sector) for nanotechnologies was 17.8 billion dollars in total[3]. As a result, the global socioeconomic value of nanotechnologies is steadily increasing, and currently, nanoscale particles have significant impacts on almost all industries and all areas of society[3]. The market for nanotechnology based electronic components and pharmaceuticals was $147 billion in 2007 and is expected to reach $2.5 trillion by 2015[19]. Advancements in the fields of nanoscience and nanotechnology have resulted in countless possibilities for consumer product applications, many of which are already being sell in store shelves and e-commerce websites. Since 2005, the Nanotechnology Consumer Products Inventory have been accounting the consumer products offered in the market, that are now 1628 consumer products available, this represents an increase of 24 percent since the last update in 2010[4]. With the fast growth of products containing nanomaterials accessible to the consumers, the Consumer Product Safety Commission has requested $7 million in funding for a new centre focused on nanotechnology in consumer products, according to a an article in Bloomberg BNA's *Product Safety & Liability Reporte*[20]. Also in European Union (EU) the research on nanotechnology takes a very special place, being a concern of many European policy initiatives. One of the biggest issues is to define how the information from nanotechnology research can and should be effectively collected, structured and presented to be further communicated to relevant EU audiences[21]. Overall, about two hundreds projects on nanotechnology have been placed in the European Commission study "Clustering, Mapping and Assessing Nanotechnology Research", conceptually referring to scientific projects and projects supporting policy-making[21]. Nanomaterials have been increasingly incorporated into consumer products, although research is still ongoing on their potential effects to the environment and human health.

In scientific literature nanoparticles (NPs) are usually defined as particles with a dimension range between 1 and 100 nm[2,3]. As particles are reduced from a micrometre to a nanometre size, the resultant properties can change dramatically. For example, electrical conductivity, hardness, active surface area, chemical reactivity and biological activity are all known to be altered[22]. The small size of the NPs, when compared to their bulk equivalents, results in a larger number of surface atoms and therefore offer increased reactivity that enhances electron transfer, efficiently binds molecular species, enhanced biological activity per given mass and easily translocate cell membranes when they are exposed to the environment[5,19]. Due to the similar size of the NPs to typical cellular components it can intrude living cells by manipulating the cellular endocytosis machinery, resulting in permanent cell damage[5]. The decrease of the particle size cause changes in structural or physicochemical properties that can lead to different biological effects of the previously reported[2]. The attractive properties of the NPs are also being utilized in advanced applications such as drug and gene delivery, biosensing, virus inhibition, and protein immobilization[19]. Many industrial sectors such as catalyst manufacturing, composite materials or passive electronic components include NPs in their processes[19]. In medicine, nanomaterials have been used as drug delivery, imaging, and the formation of bone composites. Also in the food and cosmetics industries, nanomaterials are been use to enhance the quality of their products. With the advance of the propulsion technology, nanomaterials have been shown to be a potentially useful in electronics, sensors, munitions, and energetic/reactive systems[1]. Although nanoscale materials have been produced for decades, industrial large-scale production began only in recent years[23].

For a better understanding and an improved knowledge of NPs effects on living organisms the capabilities of cells to uptake these entities, and the detailed pathways and molecular mechanisms which are involved in NPs interaction with cells require research efforts[5]. These issues have been recently recognized by international environmental, health and safety organizations in the EU and in many industrialized countries all over the world.

2.1.1 Copper oxide nanoparticles

Metallic copper have attracted attention from diverse disciplines due to the widespread use in electronics, optics, sensors, catalysts, and medical applications[18,24]**.** Copper compounds have been used as biocides over the years and with the advent of nanotechnologies, copper has been gradually used in the NPs form and applied in, e.g. hospital equipment, wood preservation, antifouling paints and antimicrobial textiles[8,9,25–27]. Cu NPs have also attracted considerable interest because of their optical, catalytic, mechanical and electrical properties, resulting in a wide range of applications in the field of metallurgy, catalysis, nano- and optoelectronics. Due to Cu high-conductivity, natural availability and market price, manufactured nanoparticles of Cu may constitute an attractive alternative to silver (Ag). Therefore, the synthesis of Cu NPs has become of great interest from a scientific as well as an industrial point of view, due to its huge potential for

replacing expensive nano silver ink in conductive inks and their printing by inkjet technology, among other applications lowering the industrial production and market costs [28,29].

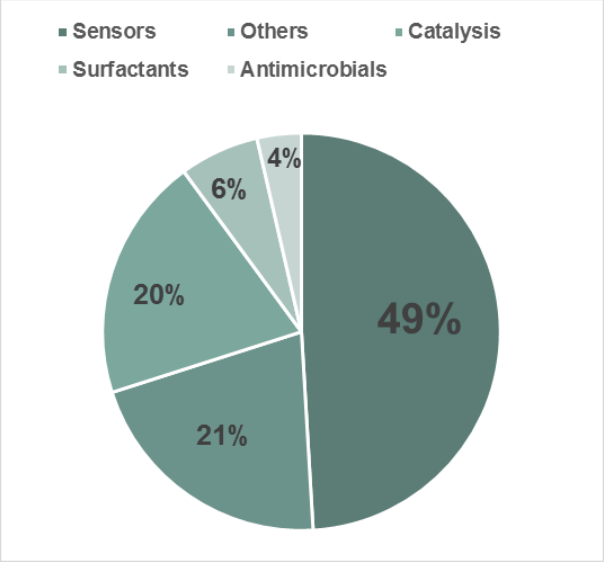

Figure 2.1 Fields of application of CuO nanoparticles
Data adapted from [3]

Copper oxide (CuO) is the simplest member of the copper compounds family and have physical properties, such as high temperature superconductivity, electron correlation effects and spin dynamics, these characteristics have brought attention for its use in several applications such as batteries, high temperature super-conductors, catalysis, gas sensors and solar energy conversion[22,30]. For example, the CuO-NPs can be used in the energy-saving industry by increase thermal conductivity and enhance the fluid viscosity, when the energy transferring fluids are filled with the CuO-NPs[30]. It can be seen in the Figure 1 that the major and most unique application of the CuO-NPs is in the technology and electronics field. These NPs are used as electronic chips, heat transfer nanofluids and semiconductors. CuO-NPs have also been used in other field, for example, in wound dressing, textiles or even cosmetics, due to their biocidal properties[3].

2.1.2 Toxicological relevance of copper in nanosize formulations

Nanoparticles and other nanomaterials have been wide spreading and steadily growing in scientific and commercial applications. Because of the proliferation of NPs uses the accumulation in the environment as well as human exposure might increase[5]. As the toxicity of NPs varies, depending on composition, coating, and weathering as well as on environmental factors, cost-efficient screening methods are needed for the toxicological analysis of synthetic NPs[9]. Therefore, similarly to pesticides, these nanomaterials should be monitored for their short- and long-term toxicological and ecological effects toward non-target species, including humans**,** to predict possible biological injuries[3,19].

Current hazard identification for risk assessment of NPs is mainly conducted with the aid of both *in vivo* and *in vitro* toxicity approaches. In nanotoxicology, *in vitro* toxicity testing for NPs has a high priority and indeed most of the studies have been conducted *in vitro*. However, the responses to NPs are known to be variable depending on cell type because of the diverse physiological functions of cells and the heterogeneous physicochemical properties of NPs[18,31]. The NPs ionic/molecular toxicity and toxicity aspects related to the nature of the material of the NPs are

the main cause of the adverse effects of NPs incorporation. For a better understanding of this phenomenon, the detailed molecular mechanisms of cellular NPs uptake have been investigate[5].

Some metals such as copper, manganese, or zinc are required in trace amounts for essential cellular functions but become toxic in excess quantities[10].The increasingly use of metal nanoparticles in various consumer products such as cosmetics, sunscreens and textiles demands a search for information on toxicity and safety of NPs[2].

CuO-NPs were shown to trigger the production of ROS, to cause DNA damage and to induce mitochondrial depolarisation in cell lines, such as in adenocarcinoma human alveolar basal epithelial cells, A549. CuO-NPs may also contribute to the development of diseases like cancer, arteriosclerosis and arthritis[8].

CuO-NPs have been used to prevent the growth of different microorganisms as bacteria, fungi and algae. The release of NPs into waste streams and further into the environment, may be a risk to the 'non-target' organisms, such as aquatic organisms and microbes[3,6]. The adverse effects of CuO-NPs toward a wide range of bacteria, mostly at concentrations between 10−100 mg/L, has been reported. However, recombinant bioluminescent sensor bacteria *Escherichia coli* responded to subtoxic concentrations of CuO-NPS (0.1mgCu/L) which induced the formation of superoxide anions, hydrogen peroxide, and single-stranded DNA[23].

As a general hypothesis for explaining the toxicity of CuO-NPs, their capacity to generate reactive oxygen species (ROS) has been suggested. Several *in vitro* studies using human lung epithelial cells (A549) have reported that CuO-NPs triggered ROS production and induced oxidative stress, mitochondrial depolarization and DNA damage [8,9]. Some studies were performed to elucidate weather the toxicity of CuO nanoparticles to *S. cerevisiae* is mediated by oxidative stress, throught the use of eight tentatively oxidative stress response-deficient strains[9]. The results indicated that CuO-NPs exerted toxicity in yeast cells via different mechanisms, beside oxidative stress. In previous studies, higher toxicity of CuO-NPs to *S. cerevisiae* than the bulk form of CuO was observed[2]

2.2 *Saccharomyces cerevisiae* as an experimental model to study CuO-NPs toxicity

The similarity between the cellular structure and functional organization of *Saccharomyces cerevisiae* and more complex organisms, positioned this unicellular eukaryotic organism as an attractive model to study molecular and cellular mechanisms[32]. Therefore, *S. cerevisiae* may also become a promising biological model for the toxicological evaluation of NPs[9]. The genome of *S. cerevisiae* was sequenced in 1996 and there are a wide variety of mutant strains available (European *S. cerevisiae* Archive for Functional analysis – EUROSCARF) for mechanistic studies, since that it has been the most exploited single cell eukaryotic[33]. The availability of systematic genome-wide mutant collections of *S. cerevisiae* (functional information available for nearly every gene[32]) is a powerful tool for the toxicological profiling of chemicals, e.g., in a high-throughput manner[32]. Easy genome-wide analysis are already implemented for *S. cerevisiae*, with a large number of experimental tools and biological material readily available[32].

In addition, the yeast is a unicellular non-pathogenic microorganism that have short generation time and can easily be cultivated in the laboratory at low cost[32]. Other advantage of *S. cerevisiae* as a model to evaluate cellular responses to metal toxicity and to infer detoxification strategies is the fact that *S. cerevisiae* senses and responds to a variety of environmental conditions, like osmotic and oxidative stress, temperature, nutrient depletion, and a number of chemically diverse toxicants[10,11].

All of these characteristics make the yeast *S. cerevisiae* a very useful first screening tool, preventing the use of animal models. It can also provide a truly global understanding of the toxicological response and resistance mechanisms to any environmental stress, being one of the most interesting systems in systems biology research and post-genomic developments[32,33]. After all, yeast remains a highly useful and unavoidable model in toxicogenomic studies, particularly for the understanding of tolerance mechanisms in depth at the genome-level [33].

2.2.1 Effects of copper stress in *S. cerevisiae*

Copper is a micro-nutrient that is essential for various vital functions, such as enzymatic processes in yeast. Depending on the available chemical form, Cu can be extremely toxic. At high concentrations, this element can cause extensive damage in yeast due to its role in the generation of ROS that can oxidize nucleic acids, proteins and lipids or to its direct and indirect effects in enzymes involved in metabolism and transport across membranes[6,12–14,34]. One of the most studied effects is the lipid peroxidation[34,35]. Other way to evaluate the ROS effect is to identify

possible DNA damages. Comet Assay is the most commonly used technique for the monitoring of DNA damage in cells[36–38].

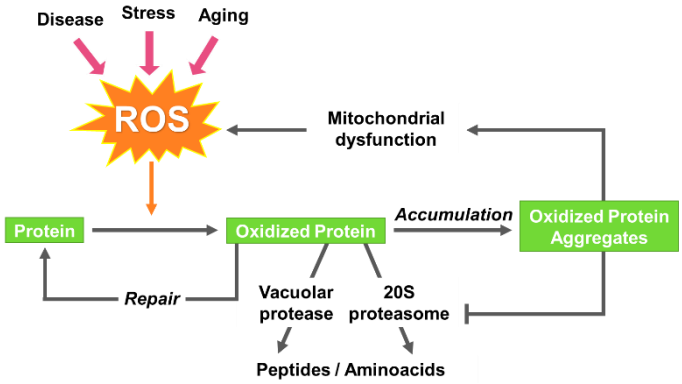

Figure 2.2 Protein oxidation and proteolysis of oxidized proteins.
(Image adapted from[39]).

ROS effects may also be studied through the assessment of protein oxidation (Figure 2.2). When ROS irreversibly damage proteins, they can be degraded by the 20S proteasome or by vacuolar proteases. However when the proteins oxidation is too extensive it cannot be degraded and tend to form aggregates that jeopardise the 20S proteasome and mitochondrial function, increasing ROS production[39]. The S-H protein functional groups, referred as thiol groups serve multiple biological functions from enzymatic catalysis to protein redox regulation. Therefor monitoring the redox state of cysteines residues can be a robust approach to study ROS toxicity. The most used methods involve differential labelling of reduced versus oxidized cysteine residues[40,41].

It is known that metallothioneins (a family of cysteine-rich proteins that bind to a variety of metals through thiolate bond clusters), have a major role in intracellular metal homeostasis, since they bind metals, these proteins serve a number of functions, including prevention of metal toxicity, as metal storage molecules, and other possible roles. Yeast, when exposed to high environmental copper levels, activates the biosynthesis of metallothioneins. This response is regulated at the level of transcriptional induction of *CUP1* and *CRS5* genes, by the CUP2, a transcription factor that binds to copper and DNA [42,43]. *CRS5* encodes a small molecular weight cysteine-rich protein with an amino acid sequence bearing all the features of a eukaryotic metallothionein. The cysteine residues, in metallothionein coordinate the metals into complexes of one or two metal binding clusters that have the high-affinity binding capacity for 8-12 atoms of copper/mol of metallothionein. [43] There are some evidences of the role for metallothioneins as an antioxidant against reactive oxygen [44–46]. Mechanisms underlying this function may include direct interception of free radicals, complexation of redox sensitive transition metals, altered zinc homeostasis or interaction with glutathione (GSH)[44]. Metallothioneins display *in vitro* oxyradical scavenging capacity. Metallothionein has been shown to scavenge hydroxyl radicals *in vitro*, because of its cysteinyl thiolate[45,46].

2.2.2 Mechanisms of copper tolerance

To preserve the delicate balance between essential and toxic levels of Cu, cells utilize sophisticated mechanisms to regulate uptake, sequestration to sub-cellular compartments and complexes, as well as detoxification[10].

In *S. cerevisiae* Cu^{+} is uptaken by two apparently functionally redundant high-affinity Cu^{+} transporters, Ctr1 and Ctr3, or a low-affinity transporter, Fet4, after Cu^{2+} is reduced at the plasma membrane to Cu^{+} [47]. As cells undergo a shift from Cu-deficient (or Cu-adequate) to high extracellular Cu bioavailability (>1 μM), apo-Ace1 regulatory protein, that is nuclear inactive, undergoes a conformational change as a result of the formation of a tetra-copper-thiolate cluster within its amino-terminal DNA binding domain. The strikingly antagonistic role of bound Cu on Cup2 and Mac1 transcription factors activities, in addition to the estimated intracellular free $[Cu^{+}]$ of approximately 10^{-18} M, suggests a complementary affinity of both transcription factors for Cu binding such that the range of activation of one transcription factor does no overlap the other[48]. Mac1 is a nuclear Cu-sensing transcriptional regulator that, under low Cu conditions, activates the *CTR1*, *CTR3* and *FRE1* genes. Thus, *S. cerevisiae*, can respond to extremely low external sources of Cu, by mobilizing Cu stores from the vacuole. This process is carried out by Ctr2, and a vacuolar-localized metalloreductase, Fre6.

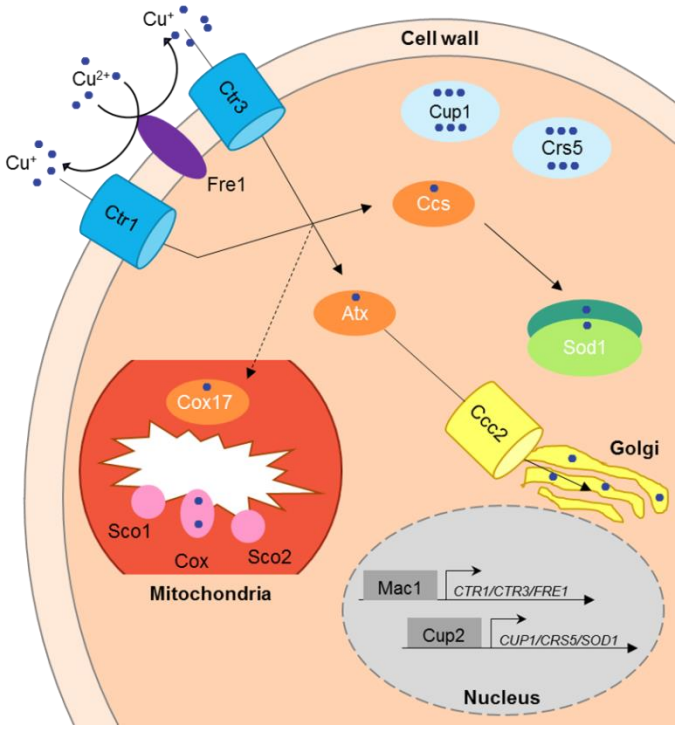

Figure 2.3 Copper homeostasis in yeast
Copper homeostasis in yeast. Ccs (oxygen and the copper chaperone) delivers Cu after reduction from Cu^{2+} to Cu^{+} by the Fre1 metalloreductase, and import by the Ctr1 and Ctr3 Cu transporters, to Sod1 to protect against oxidative stress. Atx1 is a chaperone that delivers Cu to Ccc2 (Copper-transporting ATPase) where Cu is translocated into the Golgi apparatus to be loaded onto cuproenzymes. Cup1 and Crs5 are metallothioneins that protect yeast cells from Cu toxicity. Mac1 and Cup2 are transcriptional activators that respond to Cu starvation and excess, respectively. The precise mechanisms whereby cytosolic Cu is delivered to mitochondria for loading onto cytochrome c oxidase (Cox) by Cox17, Sco1/2 and other proteins are currently unknown. (Image adapted from[47]).

When cells encounter increases in environmental Cu the expression of genes encoding Cu detoxification proteins such as metallothioneins is triggered. The *S. cerevisiae* Cup1 and Crs5 metallothioneins scavenge excess Cu by tight coordination with cysteine thiolates, which are buried from solvent, therefore poorly exchangeable and not highly reactive. Excess intracellular Cu may also favour the generation of ROS such as the potentially toxic superoxide anion (O_2^-). The enzyme Cu,Zn superoxide dismutase (Sod1) is part of the cell machinery to inactivate ROS that is also transcriptionally activated by a second Cu metalloregulatory transcription factor, Cup2. This enzyme catalyses O_2^- into hydrogen peroxide (H_2O_2) and is localized both at the cytoplasm and at the mitochondrial intermembrane space[47]. Given the role of Fe-dependent catalase in decomposing H_2O_2, one possibility is an enhanced requirement of Fe-responsive transcription factor Aft1 in mounting a response to increased oxidative burden that can equilibrate ROS in relation to H_2O_2 produced by the activity of Cu,Zn Sod1[48]. In this context, the expression of Cu detoxification genes can be complemented by the activation of *FET3* and *FTR1* genes, which encode the ferroxidase and ferrous iron (Fe) permease, respectively, involved in elemental Fe uptake.

Therefore, *S. cerevisiae* activates distinct genes in response to low and high Cu using distinct Cu-sensing transcription factors[47–49]. The interplay of these regulatory pathways enable *S. cerevisiae* to control Cu uptake and distribution and to cope with a broad range of Cu concentrations.

Although the mechanisms for of copper tolerance in yeast are well studied the mechanism of toxicity of CuO-NPs is still only partially understood.

2.3 . Nanoparticle characterization and detection in cells

The major issue in toxicity assays are to characterize NPs and to determine whether NPs are internalized by the cells.

Before any *in vitro* toxicological assay with NPs, there is a need to define particle characteristics, such as size distributions, chemical properties, among others in order to better assess the potential toxicity of NPs to biological systems. There are several techniques that can help on the evaluation of NPs physical and chemical characteristics in biological media. Chemical characteristics, especially particle dimensions can be assessed by centrifugal ultrafiltration or resin-based inductively coupled plasma spectrometry techniques. There are several techniques to characterize NPs size. The most used are the Transmission Electron Microscopy (TEM) and Dynamic Light Scattering (DLS).

2.3.1 Characterization of Nanoparticles

Dynamic Light Scattering (DLS) is a valuable technique to assess size, distribution, and the zeta potential of nanomaterials in solution[1]. DLS measures the light scattered from a laser that passes through a colloidal solution and by analysing the modulation of the scattered light intensity as a function of time, the hydrodynamic size of particles and particle agglomerates can be determined. It measures the diffusion coefficients of particles in a liquid by analysing the elastic scattering of light by the individual particles. The optical phenomenon was described by Lord Rayleigh, being usually referred as Rayleigh scattering, and occurs when the dimensions of the nanoparticles are much smaller than the wavelength of the incident light. Then the size of the particles can be parametrized by report to the wavelength of the incident light having into account the refractive index of the particle.

The DLS technique consists of analysing the fluctuations of the scattered light (suffering either constructive - light regions, or destructive - dark regions interference) from all molecules that are in the laser beam path. These light scattered patterns, which are collected by a photomultiplier in sequential time intervals, can then be correlated at each spot over time, providing dynamic information of the particles. DLS instrument measures the time dependence of the scattered light to generate a correlation function. For small time intervals particles are prevented from moving far away from initial position and the correlation is high. After long time periods elapsed the scattered intensity of the initial and final states are distinct and the correlation decays exponentially. Thus, the exponential decay can be related to the motion of the particles (Brownian motion) and therefore to the diffusion coefficient. The autocorrelation function is fitted by numerical methods by applying a number of important assumptions (monomodal size distribution, spherical particles, etc.), convert the particle diffusion coefficients value, into a number of different types of particles size distributions, such as harmonic intensity averaged particle diameter (z-average), relative percentage in class of particle diameter based on intensity, volume and number[50–52]. The diameter of a particle dispersed in a liquid medium obtained with DLS technique is that of a sphere that has the same translational diffusion coefficient as the particle being measured. The translational diffusion coefficient not only depend on the size of the particle core but also on any surface structure of the particle.

Comparing particle dimension data obtained with DLS and Transmission Electron Microscopy (TEM), the effect of aggregation state of the particles in DLS results can be estimated. In a non-agglomerated suspension, the DLS results for particle diameter agreed well with TEM size estimates. However, if the particles were agglomerated, the DLS measurement showed high polydispersity index (large variability in the particle size) and overestimation of size compared to TEM size estimate [51].

Despite the analytical limitations of DLS in resolving particles of different sizes in the same suspension, the technique can still provide the time-changes of the average NP agglomerate sizes. In this case, both the width of the particle size distribution and the mean value of the hydrodynamic diameter of the particles (polydispersion index) should be taken into account to

determine if valid data has been generated. However, the DLS technique is expedite in terms of sample type, sample preparation and manipulation, and time of analysis. All together these issues represent an unquestionable advantage over other analytical approaches, which include transmission/scanning electron microscopy, flow field sedimentation and centrifugal liquid sedimentation. Therefore, DLS technique has been extensively used to characterize NPs agglomerate in biological media in toxicity experiments.[1,7,50–54].

This technique was already been used by Murdock et al. [1], for the characterization of the agglomeration of several NPs, including Cu-NPs (40, 60, 80 nm), in different culture medium. The results enabled to see an increased agglomeration in media and decreased agglomeration in media with serum when compared with water. It was also possible to see that all solutions containing Cu-NPs, were initially at similar agglomerate sizes, approximately 380 nm. As time increased, each solution produced larger agglomerates with the trend being logarithmic in nature.

Everett et al. [54], studied the potential effects that the formation of $Zn_3(PO_4)_2$ crystallites may have on cell viability. In this study DLS was used to measure particle/agglomerate zeta potentials and average ZnO agglomerate sizes ranging from hundreds of nanometers down to individually dispersed NPs, thereby providing an ex situ estimate of agglomerate size and surface charge prior to being applied to the cell culture environment. ZnO agglomerates larger than 1.5 μm were not measured with DLS, because their sedimentation rates prohibited accurate measurement of their size distributions; therefore, their size was estimated in a batch sedimentation cell using an optical microscope.

Cascio et al. [50] has used DLS, among others techniques, to give complementary size information about suspensions of silver nanoparticles (AgNPs) in the size ranges of 20−100 nm. The technique provided quantitative particle size distribution of monomodal suspensions of AgNPs whereas it failed to identify bimodal suspensions of AgNPs particularly in the case of mixtures containing 40 and 60 nm NPs and 40 and 70 nm NPs. Hydrodynamic diameters of intermediate value between the two real sizes were systematically closer to the biggest particles, evidencing an overestimation of the average size.

2.3.2 Imaging cellular uptake of nanoparticles

So far TEM has been the technique of choice for high-resolution imaging of subcellular structure, in order to estimate sizes and shapes of NPs and confirm their internalization by cells. However, this approach presents numerous technical difficulties in what concerns the analysis of individual NPs and is not representative, as only a thin section of the cell or tissue is analysed.

New imaging approaches have recently emerged offering sub-cellular resolution. Those which are based on optical microscopy are limited by the light diffraction limit (approximately 250nm), either requiring the use of fluorescent probes to tag NPs or the NPs under study has to be fluorescent. Although some studies have been made using confocal optical microscopes or other

modalities, multiple scattering is still a limitation to achieve adequate depth resolution, to resolve NPs localization accurately [15].

The microscopy techniques based on accelerated ion beams are attractive for detecting internalization of NPs by cells as they enable sub-diffraction depth resolution allied to relatively good sub-micron lateral resolution images of elemental distributions. The depth profile can be assessed by accounting the energy loss of the incident beam, usually protons or alpha particles (nucleus of helium atom), when it is backscattered by an atom encountered in its path through the cell. Depending on the mass of the projectile and its energy it is possible to achieve depth resolutions <100nm for a biological matrix[15].

Nuclear microscopy, is a technique based on focused MeV ion beams to micrometer dimensions that can deliver images of the morphology of a tissue or cell and the correspondent elemental distributions in real-time. In a nuclear microscopy set-up the beam is focused using electromagnetic lenses and raster through the sample in a predefined pattern. For each position of the beam (x,y,z coordinates) corresponds an image element or pixel. The detection of beam particles, usually protons, that are scattered, and photons or electrons produced by the interaction of the accelerated particles with the atoms in the specimen different images of the sample morphology and composition can be obtained[16,17].

In nuclear microscopy, the detection of scattered and transmitted protons, induced X-rays, emitted secondary electrons, among others, can be done simultaneously and the images produced display features of the sample that cannot promptly be imaged by other techniques[17].

Using nuclear microscopy techniques, trace elemental information can be obtained providing not only the chemical composition of the sample, but also 2D- elemental maps[16,17,55]. The incoming accelerated protons have enough energy to ionize atoms resulting in the emission of a characteristic X-ray. The energy of X-rays emitted are unique for each element, enabling to identify several elements present in the sample. This is the basis of Particle Induced X-Ray Emission (PIXE) technique, which has outstanding analytical sensitivity and quantitative precision (1–10 μg/g on a dry weight basis), especially for transition elements which are essential trace elements in biological tissues[17].

Other technique available in nuclear microscopy is Rutherford Backscattering Spectrometry (RBS). This technique is based on the energy loss by the incident particles (protons or alpha particles) during its path in and out of the sample. This technique enables the measurement of the depth variations of the specimen for an estimation of matrix composition, meaning that data on the matrix elemental composition and on the thickness of the sample is obtained [17]. The energy of protons or alpha particles that are backscattered from atomic nuclei in the sample are dependent on the nucleus involved in the collision. The energy loss measurements reflect the position of the atom in the matrix and can be expressed in terms of thickness. This will enable to determine the depth at which NPs are found in the cell, providing an adequate mass discrimination between the metal associated to NPs and other elements present in the specimen. RBS can also

be used to normalize PIXE spectrum, using the estimative of matrix composition obtained. This will allow to determine 2D quantitative maps of the elemental distributions.

STIM technique allows the analysis of the energy loss of particles that are transmitted across sample. This technique is mostly used to determine specimen density. The density variations of the sample cause variations on the energy loss of the transmitted protons that did not suffer nuclear backscattering collisions. Sub-cellular scale resolution images (<0.5µm) can be obtained routinely by the measurement of density variations[17]. This can provide structural and morphological information of cells and tissues that can be used to correlate with elemental distribution images.

Together these three methods, which can be carried out either simultaneously or successively on the same sample region, are well adapted to the measurement of the major, minor, and trace element concentrations in most biological tissues and cells. The main advantages of use of these methods are: a rather simple sample preparation without fixation and staining, a large observable area with the option to zoom into regions of interest, the easy quantification of concentrations at a level of sensitivity of a few parts per million.However, the disadvantage of nuclear microscopy is that individual nanoparticles cannot be resolved in common set-ups[55].

Nuclear microscopy techniques proved to be a unique tool in metal permeation studies as *in vivo* material can be assessed and rigorous results can be provided as long as sample preparation and quantitative analysis are strictly controlled, allowing qualitative imaging of the distribution, and quantitative determination of intracellular concentrations[56]. The nuclear microprobe technique is a powerful tool enabling qualitative imaging of the distribution, and quantitative determination of metals in biological samples. The procedure allies a good lateral resolution of the order of the micrometer to excellent detection limits of the order of microgram/g (dry weight basis). In addition RBS allows to assess the depth at which specific feature is found, such as NPs. This positions this technique in the forefront of microscopy modalities for studying the interactions of NPs and single cells[55].

Several studies had been carried out for assessing metal distributions in single cells using nuclear microscopy. The toxicity and tolerance to metal overload was studied using diatoms *Coscinodiscus eccentricus.* The changes in cellular contents for Ni, Cu and Zn and the compartmentalization of These metals in whole diatom cells enable to estimate consequences to cellular toxicity and metal fate in the marine environment (Figure 2.4)[57].

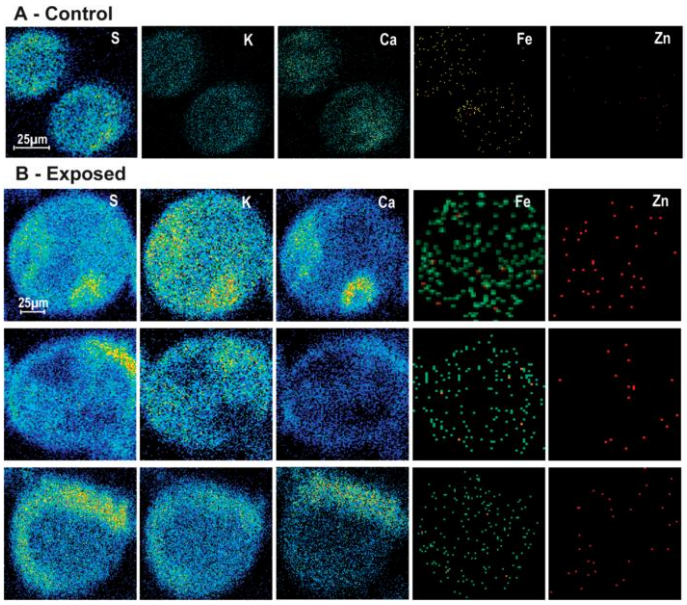

Figure 2.4 PIXE maps of spatial distribution of S, K, Ca, Fe and Zn in individual *Coscinodiscus eccentricus* cells.
Content gradient is represented by a colour dynamic scale: high content – red, to low content – blue (reproduced from[57]).

Using specific focusing conditions allied to a selective choice of beam energy imaging of AuNPs in HeLa cells was demonstrated[58]. Taking advantage of the lateral resolutions of ~25 nm capabilities a high resolution image of cell density and gold NPs distribution was obtained (Figure 2.5 a and b), enabling individual NPs detection. By exploring the depth profiling capabilities of RBS technique, the depth at which gold NPs were detected coulb be determined. Anestimated depth resolution ~65 nm was obtained from the RBS data (Figure 2.5 c and d). This study demonstrate for the first time the ability of nuclear microprobe techinques to discriminate where the NPs are at the surface or inside the cell. Thus internalization of Au-NPs by cells was inequivocally proved[58].

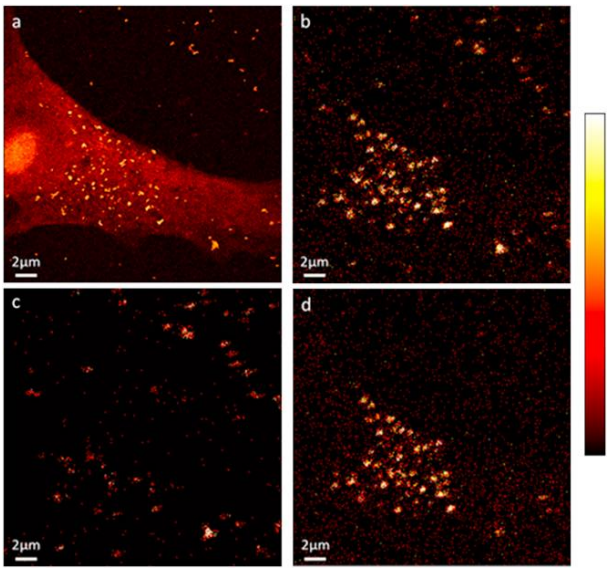

Figure 2.5 Images of HeLa cells culture in an environment of AuNPs obtained with nuclear microscopy techniques.
(a) STIM image of a HeLa cell cultured, where cell boundaries and nucleus can be depicted. (b) Total RBS image of the same HeLa shown in a) where AuNPs can be identified. The AuNPs distribution are confined to the cell (c) Cell surface RBS Au image revealing the presence of AuNPs on surface layers of the HeLa cells. (d) Subsurface RBS Au image revealing AuNPs that were internalized by the HeLa cell. (Reproduced from[58]**)**

3 Materials and methods

3.1 Copper solutions

A solution of CuO-NPs (CuO 99+%, 30-50 nm) with a relation of 0.2248 gCu/gNPs (determination carried out by R. Domingues, Centro de Química Estrutural, IST. Unpublished data.) were purchased from Nano Amourphous, was used in this study. The CuO-NPs stock solutions (67.5 mgCu/mL) were prepared in ultrapure water with 18 MΩ.cm resistivity (MilliQElement®, Millipore), sonicated in an ultrasonic bath, for 30 min (VWR B-3001 Leuven, Malaysia) and stored in the dark at room temperature. CuO-NPs intermediary solutions whenever needed were prepared in Teflon container and also prepared with ultrapure water (MilliQElement®, Millipore), in order to avoid contaminations.

A copper sulfate ($CuSO_4$) solution was used as the equivalent salt of CuO-NPs (Cu^{2+}), serving as a positive control to experiments with NPs. The $CuSO_4$ solution with a concentration of 160 gCu/L, was made through the addition of Cupric Sulfate $CuSO_4 \cdot 5H_2O$ (Sigma-Aldrich, USA) and deionized water. An intermediary solution of $CuSO_4$ (16 gCu/L) was used for the preparation of the solutions used on the assay.

3.2 Strains and growth conditions

The parental *Saccharomyces cerevisiae* strain BY4741 (MATa, his3Δ1, leu2Δ0, met15Δ0, ura3Δ0) and the derived single deletion mutant BY4741_Δ*cup2*, used in this work, were obtained from the EUROSCARF collection. Minimal growth medium MM4 used contains (per litre): 1.7 g yeast nitrogen base without amino acids or $(NH_4)_2SO_4$ (Panreac, Spain), 20 g glucose (Merck, Germany), 2.65 g $(NH_4)_2SO_4$ (Panreac, Spain), 20 mg histidine (Merck, Germany), 20 mg methionine (Merck, Germany), 60 mg leucine (Sigma-Aldrich, USA) and 20 mg uracil (Sigma-Aldrich, USA). Solid media were obtained by the addition of 20 g/L agar (Iberagar, Portugal). The growth media pH was adjusted to 4.5) using HCl or NaOH. *S. cerevisiae* strains were maintained at -80 ºC in appropriate media supplemented with 30 % glycerol (v/v). Yeast strains were streaked onto agarized plates, cultivated at 30 ºC until growth in the plates was observed and then kept at 4 ºC until further use.

The susceptibility of the parental strain BY4741 and derived deletion mutant to toxic concentrations of CuO-NPs and $CuSO_4$ was assessed by comparing growth curves and determining the concentration of viable cells in MM4 medium. Cells (wild type and mutant strains) growing in pristine MM4 culture medium (without CuO-NPs or $CuSO_4$ supplementation) were taken as controls. *S. cerevisiae* cells were grown in MM4 medium until reaching an optic density at 600nm (OD_{600nm}) corresponding to the exponential phase (OD_{600nm} of 1.5 ± 0.1). Then cells were re-inoculated by filtration (Membrane filters white, 0.2 µm, Whatman™, ME24/21ST), at an $OD_{600\ nm}$= 0.5 ± 0.05, in 50 ml of fresh medium, either or not supplemented with different

concentrations (ranging from 6 to 100 mgCu/L) of CuO-NPs. Cells were grown at 30ºC with orbital agitation (250 rpm), and growth was followed by measuring culture OD_{600nm} during batch cultivation. Viability was determined by colony-forming units (CFU) counts after 3 days of incubation at 30 ºC on MM4 agar plates. Viability assays were performed using cell aliquots taken throughout growth. 100 µl from 1/10 serial dilutions were inoculated in MM4 agar plates. The protocol was also performed in cells supplemented with $CuSO_4$, with a range of concentrations of 0.06 mgCu/L to 200 mg Cu/L.

3.3 CuO-NPs characterization using Dynamic Light Scattering (DLS)

A Malvern Zetasizer Nano-ZS instrument (Malvern Instruments Ltd, England), with temperature control, was used to determine the particle size distributions. The equipment uses the Dispersion Technology Software (DTS) (V4.20) for data collection and analysis. The mean particle diameter is calculated by the software from the particle distributions measured through the Z-Average (intensity harmonic for the average particle diameter) and Intensity Mean (diameter class average, most representative in terms of intensity); the polydispersity index (PdI) given is a measure of the size ranges present in the solution (Malvern, Instruments Ltd., 2005). Samples were vortexed to provide a homogeneous solution, and then 1ml was transferred to a square cuvette for DLS measurements. The experimental set-up used in this work is illustrated in Figure 3.1.

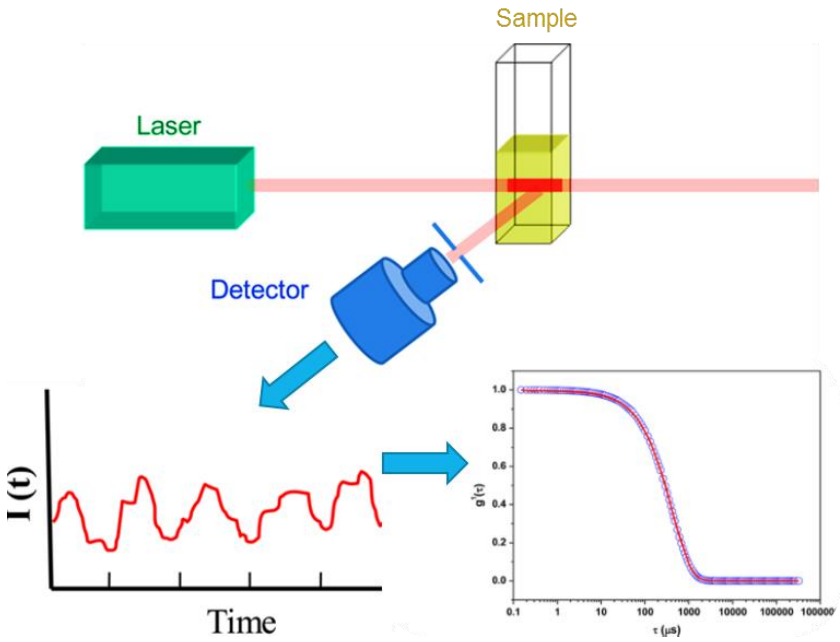

Figure 3.1 Schematic representation of Dynamic Light Scattering (DLS) technique.
The intensity of the light scatter by the sample is recorded by a photomultiplier detector. The time dependence of the light intensity is given by a correlation function G (τ) that can be linked to the particle size. (reproduced from[52]).

3.3.1 Calibration procedure

For the DLS calibration procedure, polystyrene standard spheres of 0.4 μm and 0.69 μm diameter (Bangs Laboratories, Inc., USA) were used to validate conditions of analysis including instrument parameters for particle size determination. Suspensions of approximately 10^7 beads/mL obtained by dilution of the standard suspension in 18 MΩ.cm ultrapure water (MilliQElement®, Millipore) were used for DLS analysis. To avoid contamination only polyethylene and Teflon containers were used in preparing the suspensions, which were previously cleaned with HNO_3 (50% v/v), rinsed with 18 MΩ.cm ultrapure water (MilliQElement®, Millipore), and dryed in a laminar flow chamber. The stock and intermediate solutions were prepared and stored in Teflon containers.

3.3.2 Analysis conditions

In order to establish the optimized analytical conditions for the characterization of CuO-NPs, different concentrations of CuO-NPs were tested in aqueous and MM4 culture medium. The tests were performed with aqueous suspensions and MM4 medium containing CuO-NPs concentrations from 6 mgCu/mL to 30 mgCu/L to comply with concentrations used in cell experiments. A range of equilibration time (t_{eq}) from 5 to 120 s and a range of acquisition times ($t_{analysis}$) from 15 to 90 s were tested. These tests allowed to establish the most adequate conditions of analysis, such as times of suspension equilibrium and acquisition, optical density correction, NPs concentration, among others.

3.3.3 NPs agglomeration assessment

The study of the agglomeration of the CuO-NPs over time in culture medium (MM4) was performed in parallel assays without cells carried out simultaneously to the exposure assays. Temperature and agitation conditions were kept constant in all experiments. The samples analysed for the agglomeration study, were collected at the beginning of growth (0h), along the growth curve up to 48 hours. For exposure tests with high concentrations of CuO-NPs, samples were diluted to a suitable proportion that ensures CuO-NPs concentration less than 20 mgCu/L. The polydispersion index (PdI) and the mean average size of the distribution (Z-average) were the parameters used to estimate the NPs agglomeration index. The agglomeration index represents the changes in average distribution of CuO-NPs particle size (Z-Average) over time relative to the initial time (t=0). The index was calculated as the ratio of the Z-average value at any time relative to the Z-average value for t=0.

3.4 Determination of protein free thiol groups

Protein thiol labelling and detection was based on the methodology proposed by Kim et al. [41]. The method allow the detection of proteins that contain sensitive cysteine residues, providing the identification of proteins that are oxidized in response to a variety of extracellular agents.

Yeast cells were harvested at exponential phase of growth (6 h) by centrifugation at 6000 rpm, 4 °C during 5min. Cell pellets were resuspended in 500 µL Tris buffer (Tris-HCl 10 mM; pH 6.5 adjusted with NaOH 1 M) containing protease inhibitors (10 mg/mL leupeptine; 1 mg/mL pepstatine A; 20 mg/mL aprotinine; 2 mg/mL trypsin/quimotrypsin inhibitor; 1.5 mg/mL benzamidine; 1 mM PMSF, all obtained from Sigma-Aldrich, USA) and Maleimide– PEG2–biotin (Pierce, USA), added to a final concentration 100 times higher than the estimated protein concentration. Cells were disrupted by vortex in the presence of an equal volume of glass beads (425-600 µm of diameter) (Sigma-Aldrich, USA) for 5 min, alternating 30 s of vortexing with 30 s in ice. Cell lysates were incubated for 45 min at room temperature to allow alkylation by the maleimide–PEG2–biotin reagent of the nonoxidized protein thiols available at pH 6.5. The labeling reaction was quenched by the addition of dithiotreitol (DTT) (Sigma-Aldrich, USA) to a final concentration of 20 mM and the mixture was centrifuged at 5,500×*g* for 10 min. The resulting supernatant was collected and its protein concentration was determined using Pierce™ BCA Protein Assay Kit (Thermo Fisher Scientific, USA). Samples containing equal protein amounts (5 mg) were subjected to SDS-PAGE (10% polyacrylamide), transferred to nitrocellulose sheets, and incubated with horseradish peroxidase-conjugated streptavidin (Sigma-Aldrich, USA) 1:100,000. The detection of protein thiol bound maleimide–PEG2–biotin was achieved through chemoluminescence using the ECL Western blot kit (Amersham).

3.5 Quantitation of Cu in yeast cells with Nuclear Microscopy

3.5.1 Sample preparation

An aliquot of 5 µl of the cell suspension was rapidly deposited on a 1.5 µm polycarbonate foil (Figure 3.2), quench-frozen at – 80 °C, and finally, cells were allowed to dry at – 25 °C in a cryostat. The procedure ensured cellular integrity[56,57]. Cell quality and localization in the target for analysis was checked under the light microscope, prior to analysis.

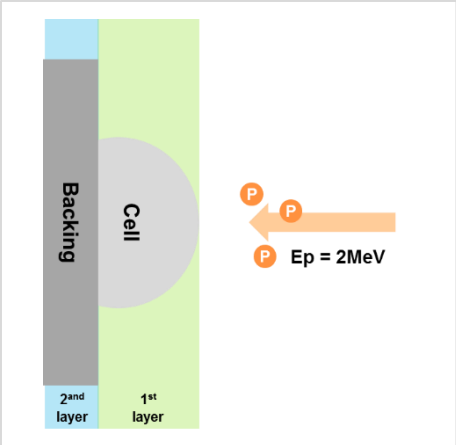

Figure 3.2 illustration of the geometry used in the analysis. Proton (P) beam striking a sample (Cell), deposited onto a 1.5 µm polycarbonate foil (Backing). The cell and the backing are independent layers of analysis (see text for more details).

3.5.2 Nuclear Microscopy technique

The nuclear microscopy technique is installed at the Van der Graaff accelerator of the Centro Tecnológico e Nuclear of IST. Analyses were carried out in vacuum using a proton beam of 2 MeV energy with a current of 100 pA. The lateral resolution under this irradiation conditions were typically <= 3 μm. For lower count rates (low current mode < 100 pA) used for density measures the lateral resolution drop to sub-micron dimension. The experimental set-up used in this work can be depicted in Figure 3.3.

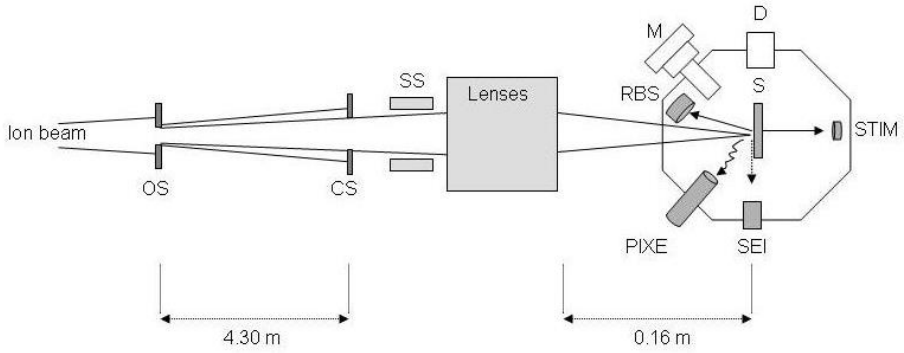

Figure 3.3 Lay-out of a nuclear microprobe installed at ITN.
The distances between object slits – OS and collimation slits CS and between the focusing lenses system exit and focus plane (S) where the sample is positioned, are given; SS – scanning system for beam deflection. The chamber configuration (Oxford Microbeams Ltd) enables a microscope (M) and several detectors for X-rays (PIXE), for backscattered particles (Si surface barrier detector for RBS) for transmitted particles (collimated windowless photodiode for STIM) and an additional position – D, for other detector. Reproduced from[17].

Particle induced X-ray emission (PIXE), Rutherford backscattering spectrometry (RBS), and scanning transmission ion microscopy (STIM) were used simultaneously to obtain morphological and quantitative elemental distribution data. The PIXE technique provides information on both major and trace elements. The RBS enables the measurement of matrix composition, depth variations and sample stoichiometry. The normalization of the PIXE through RBS allows quantitative measurements of elemental concentrations. STIM provides measures of density variations, and high-resolution images (<0.5 μm) of the sample morphology[17]. The geometry used in the analysis of yeast cells and the typical spectra obtained for each technique are represented in Figure 3.2 and

Figure 3.4, respectively.

Maps of the scanned cells were generated assigning the various detector signals to a digital X–Y positional coordinate. The relative amount measured is represented by a colour gradient. The size of the micro-areas scanned was between 26 μm x 26 μm and 106 μm x 106 μm. Point analyses across cells rendering concentration profiles were produced. Acquisition and processing of data were performed using OMDAQ and DAN32 programs, respectively[59,60].

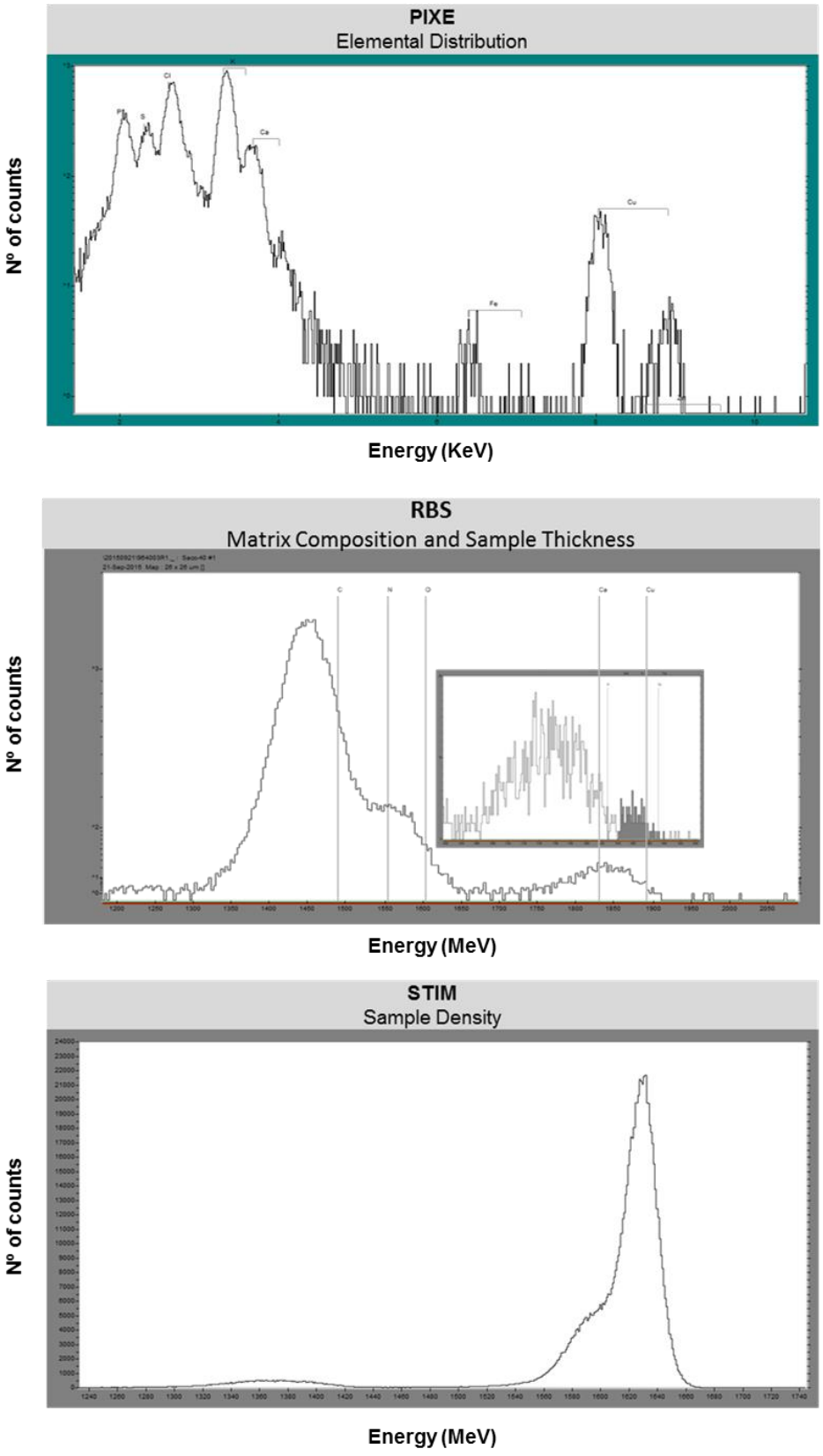

Figure 3.4 Typical spectra obtained for the three nuclear microprobe techniques used: spectra of detected X-rays (PIXE), backscattered (RBS) and transmitted (STIM) particles.

3.5.3 Imaging and quantitating Cu in *S. cerevisiae*

The methodology of analysis included cell imaging for density variations, major, minor and trace elemental maps, and elemental concentration determination.

Images of density variation enabled fast identification of cells in scanned areas. By analysing the energy loss of the transmitted beam, individualized cells, monolayers and agglomerates can be identified as density changes for cell assembly and overlap. Images of elements detected by PIXE and RBS techniques can also be produced by selecting the region of the spectra corresponding to each element.

As PIXE is a multi-elemental technique, several elements can be detected simultaneously. Therefore, physiological elements, such as phosphorus (P), sulphur (S), chlorine (Cl), potassium (K), calcium (Ca) and iron (Fe), among others, can be detected in a single run. The number of X-rays detected for each element corresponded to the number of atoms present that were ionized in a sample volume under the beam spot. If the mass of this region is known the method becomes fully quantitative. This can be done using RBS technique simultaneously with PIXE, to estimate the sample mass under the beam[60]. The energy of the backscattered particles (protons), which suffered elastic interaction with the sample atoms enabled to identify major constituents of the sample, that is to say the matrix constituents, because the energy loss in the impact depend on a kinematic factor and on the mass ratio of the projectile and atom nucleus. The analysis of the RBS spectra enables to estimate the proportion of matrix elements, such as C, N, and O and express the results in units of weight (or atoms) per area. Therefore the number of X-rays detected with PIXE can be normalized to mass using the RBS matrix estimation, rendering concentration values for any element detected in the sample. Concentrations are usually expressed in mg/g on a dry weight basis.

3.5.4 Determining NPs depth profile in cells

To investigate the internalization of the CuO-NPs by the *S. cerevisiae* strains, the depth profiling capabilities of the RBS technique were explored. A proton beam of 2.0 MeV was used. The methodology consisted of dividing the barrier on RBS spectra, which correspond to Cu, in energy intervals to estimate the amount of surface and internal Cu on the yeast cells (Figure 3.5).

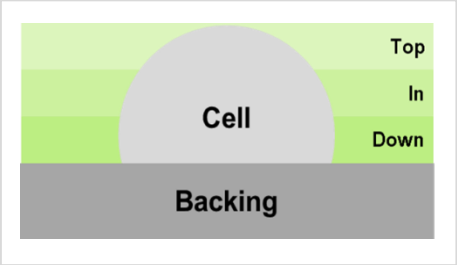

Figure 3.5 Illustration of the layers defined with RBS to analyse the Cu profile in the yeast cells.

This method was validated using a simulation of the matrix estimation obtained for *S. cerevisiae* cell (non-exposed) and the detection resolution to discriminate Cu presence at different depths. Thus, a Cu layer was inserted in the estimated matrix (C8.84 N1.06 O0.9 Na0.04 K0.02 P0.12 Wt%) from the surface to deeper layers in intervals of approximately 50 nm. The cell thickness was assumed to be of 1 μm. The thickness interval corresponding to the backscattered energies between Ca and Cu was used. The depth resolution for protons was found to be of the order of 150-200 nm, which is enough to discriminate between the surface of the cell and the interior of the cell. The methodology can be applied safely as there are no other elements present in cell which can significantly interfere with the Cu barrier, having into account the realistic limit of 1 μm thickness for cells.

3.5.5 Statistical analysis

The cell elemental concentration data was obtained from serial points taken across cells. The elemental concentrations in control cells and cells exposed to Cu, either $CuSO_4$ and CuO-NPs were summarized as median and 25% and 75% interquartiles (IQ). The elemental concentrations in the different experiments using *S. cerevisiae* cells (wild type and the mutants) non-exposed and exposed to Cu were compared applying Kruskal-Wallis non-parametric test. Tests were considered significant when $p \leq 0.05$. Statistical analyses were performed with SPSS® Software version 22 (IBM Corp.).

4 Results

4.1 CuO-NPs characterization

The Dynamic Light Scattering (DLS) technique was used to assess the size and aggregation of the CuO-NPs in the stock suspensions and in culture medium. Parameters of analysis, such as, equilibration times (t_{eq}) and acquisition times ($t_{analysis}$) were adjusted using standard spheres of 0.4 μm and 0.69 μm diameter, as mentioned in 3.3.1. The results are summarized in Table 4.1. The assays were recorded at 25 ± 0.1 °C, in duplicate. The analyses were performed with an equilibration step of 20 s and 120 s before each measurement, acquisition time was 10 s and 90 s and the software was set into automatic acquisition mode.

Table 4.1 DLS analysis of polystyrene standard beads in aqueous suspension
The average hydrodynamic diameter of particles calculated by the Z-Average Intensity Mean and polydispersion index (PdI). The PdI values represent the dispersion of sizes present in the sample.

PB size (μm)	t_{eq} (s)	$t_{analysis}$ (s)	Z-Average (d,nm)	PdI	Intensity Mean (d,nm)
0.4	20	10	424 ± 7	0.05 ± 0.03	443 ± 8
	120	90	417 ± 5	0.03 ± 0.02	430 ± 1
0.69	20	10	801 ± 57	0.09 ± 0.06	825 ± 50
	120	90	652 ± 77	0.19 ± 0.06	640 ± 66

The results are similar in both experimental conditions (different t_{eq} and $t_{analysis}$), showing that it is possible to execute this technique with both t_{eq} and $t_{analysis}$. However for t_{eq}= 120 s and $t_{analysis}$= 90 s results obtained were closer to the size limits indicated by the manufacture. The PdI values obtained, indicate a monomodal distribution of the standard spheres (PdI <0.2). The average particle size (Z-Average and Intensity Mean) obtained is within the size limits indicated by the manufacturer. The differences observed between these two parameters were not significant, as can be inferred by comparing the values of Z-Average and Intensity Mean indicated in Table 4.1.

The optimization of the experimental conditions for the analysis of the CuO-NPs were carried out using aqueous suspensions of CuO-NPs and biological medium (MM4) (Table 4.2 and Table 4.3).

In the Table 4.2 is displayed the analysis of CuO-NPs in aqueous suspension. It was established that the best conditions of analysis were for t_{eq} of 120 s and $t_{analysis}$ of 90 s per measure (run), since the best results were obtained under these conditions (Table 4.2).

Table 4.2 DLS analysis of CuO–NPs in aqueous suspension.
The average hydrodynamic diameter of particles calculated by the Z-Average Intensity Mean and methods; PdI polydispersion index. The PdI values represent the dispersion of sizes present in the sample.

CuO-NPs (mgCu/L)	t_{eq} (s)	$t_{analysis}$ (s)	Z-Average (d.nm)	PdI	Intensity Mean (d.nm)
25	120	60	463 ± 34	0.41 ± 0.02	363 ± 40
		90	453 ± 10	0.40 ± 0.01	348 ± 24
	180	60	421 ± 12	0.39 ± 0.01	363 ± 24
		90	1257 ± 601	0.74 ± 0.24	371 ± 74

The behaviour of CuO-NPs in the biological medium was studied taking into account the results obtained in preliminaries tests. Suspensions samples with 6 and 20 mgCu/L of CuO-NPs were analysed in MM4 growth medium (Table 4.3). The results were only satisfactory, taking into account the PdI values. However the average diameter of the nanoparticles increased, which suggests modification of the particle surface when in MM4 medium. Therefore differences were observed between the Z-Average and Intensity Mean values, regardless of the concentration of nanoparticles in the biological environment, reflecting the presence of populations with different particle diameters of the NPs in the suspension.

Table 4.3 CuO-NPs suspensions analysis in MM4 in liquid medium.
The average hydrodynamic diameter of particles calculated by the Z-Average Intensity Mean and methods; PdI polydispersion index. The PdI values represent the dispersion of sizes present in the sample.

CuO-NPs (mgCu/L)	t_{eq} (s)	$t_{analysis}$ (s)	Z-Average (d,nm)	PdI	Intensity Mean (d,nm)
6	120	90	1028 ± 103	0.51 ± 0.07	643 ± 35
20	120	90	1651 ± 113	0.33 ± 0.09	1386 ± 166

The measured average size of NPs diverge from manufacturer specifications. The broadening of size distributions values reflect both the aggregation of NPs and the difficulty of correcting for optical absorption of CuO-NPs, which interferes with the efficient detection of the particles under the laser beam. However, as long as PdI values drop below acceptable quality measures, relative comparisons between samples are still possible as CuO-NPs absorption is a constant parameter.

The effect of sample contamination in DLS results can be inferred from data listed in Annex 8.1.1. The use of flasks and containers traditionally used in cell cultures rendered erratic values of particle size distribution and systematically high values of PdI (~ 0.5 or higher) and large discrepancy between the Z-Average and Intensity Mean values with Mean Intensity/Z-Average

ratio below 0.61. This indicates dispersion of the NPs sizes, with the presence of large particles, which may be due to the presence of impurities in the samples. To mitigate the contamination sources polyethylene or Teflon material thoroughly cleaned was used in all experiments.

4.1.1 Study of aggregation of CuO-NPs with time

To assess the aggregation of the nanoparticles during the time period of the CuO-NPs exposure tests in *Saccharomyces cerevisiae*, samples were analysed in MM4 medium at concentrations from 10 to 40 mgCu/L. The tests were performed under the same experimental conditions of the yeast incubation. For all conditions tested, the Z-Average Intensity Mean and PdI values obtained indicated a monomodal distribution. The data are presented in Annexes 8.1.3 and in Table 8.3. The alterations on the agglomeration index of the CuO-NPs are represented in Figure 4.1.

Table 4.4 CuO-NPs agglomeration index range, in MM4 liquid medium.
The agglomeration index range represents the maximum and minimum of agglomeration index obtain in different samples with the same concentrations of CuO-NPs. The agglomeration range represent the difference of the CuO-NPs size distribution (Z-Average). The size distribution of the CuO-NPs were monitored by DLS for 48 hours.

CuO-NP (mgCu/L)	Agglomeration Index Range (%)
10	2.6 - 60.8
15	2.0 - 40.0
20	1.5 - 30.31
40	1.0 - 50.3

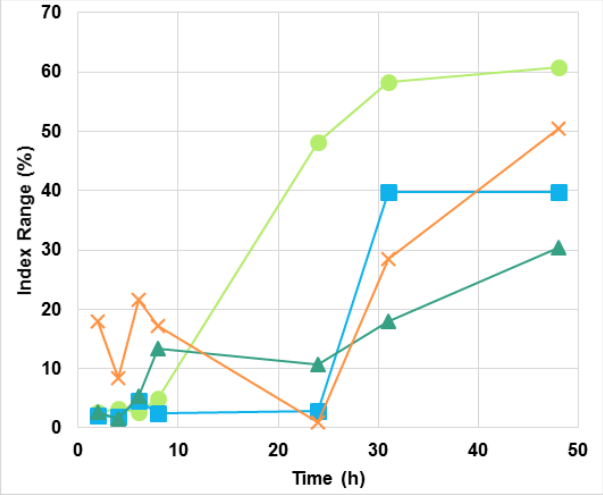

Figure 4.1 Changes of CuO-NPs agglomeration index, in MM4 liquid medium. The agglomeration index represent the ratio of the average distribution of particle size (Z-Average) of CuO-NPs relative to t=0. The size distribution of the CuO-NPs were monitored by DLS, for 48 hours. 10 mgCu/L (●), 15 mgCu/L (■), 20 mgCu/L (▲) and 40 mgCu/L (×) were the concentrations of CuO-NPs analysed.

The agglomeration indexes were dependent on the CuO-NPs dose. Although, the agglomeration index values showed that the NPs size distribution remained stable for 8 hours, after this period, the distribution broadens, indicating an increase of average distribution of particle sizes. Increases of agglomeration index were obtained for concentrations lower than 20 mgCu/L CuO-NPs. After 24 hours the changes of agglomeration index increased significantly (Figure 4.1), indicating that the quality of results can no longer be assured, as suggested by discrepancies in Z-Average and Intensity Mean (see Annexe 8.1.3, Table 8.3). The values obtained for the 10 mgCu/L of CuO-NPs displayed higher values of the average distribution of particle size, throughout the experiment period of time, in comparison to the values obtained for the other CuO-NPs concentrations tested (Figure 4.1) resulting on higher agglomeration index values (2.6% to 60.8%) (Table 4.4). The higher agglomeration rates obtained for 10 mgCu/L concentration may reflect the low average mean for the distribution obtained at t=0 (see Annex 8.1.3), meaning less aggregates of NPs relative to higher concentration levels tested. This may justify the slower rate of NPs aggregation for higher levels of NPs concentrations, as more aggregates exist in suspension at initial times of analysis (Table 4.4).

4.2 Copper susceptibility of *Saccharomyces cerevisiae* strains

4.2.1 The effect of $CuSO_4$ in *Saccharomyces cerevisiae* strains growth

Exposure tests of $CuSO_4$ in *S. cerevisiae* had the purpose to estimate inhibitory copper concentration levels of yeast growth that can be taken into account in the tests with Cu nanoparticles. The use of a Cu salt ($CuSO_4$) ensures that Cu is mainly in the ionic form in an aqueous solution and available for cell uptake.

The monitoring growth of yeast *Saccharomyces cerevisiae* BY4741 in the presence of $CuSO_4$ was performed by measuring the optical density at 600nm (OD_{600}nm) over 30 h of incubation (Figure 4.2). A broad level of concentrations from 0.06 mgCu/L up to 200 mgCu/L of $CuSO_4$ were studied. It was taken as a control, cultures of *S. cerevisiae* without the addition of $CuSO_4$.

Cultures exposed to concentrations up to 40 mgCu/L $CuSO_4$ do not induce growth arrest and the culture shows a slightly inhibited growth behaviour when compared to the control conditions (Figure 4.2). Cultures exposed to 60 mgCu/L $CuSO_4$ show a decreased specific growth rate (Figure 4.2), compared with the control cultures or to cultures exposed to lower $CuSO_4$ concentrations, but they are not completely inhibited. When exposed to 200 mgCu/L $CuSO_4$, the cultures exhibit an inhibited growth, at least during the time of the assay (30 h) (Figure 4.2).

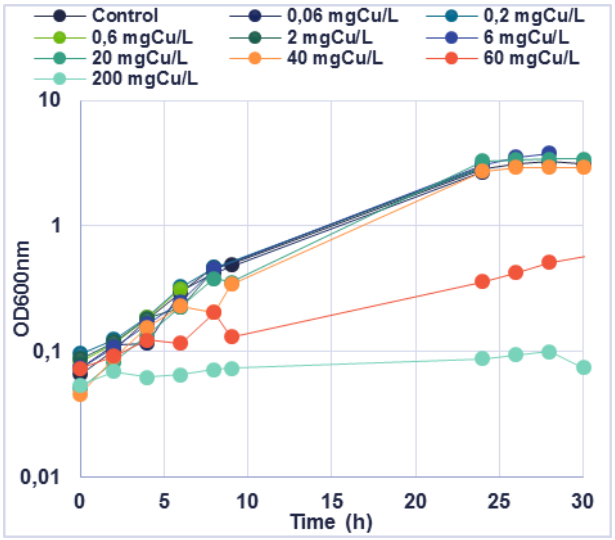

Figure 4.2 Growth curves of *Saccharomyces cerevisiae* BY4741 in a MM4 liquid medium (pH 4.5) supplemented with different concentrations of $CuSO_4$. Growth curves of cultures supplemented with 0.06, 0.2, 0.6, 2, 6, 20, 40, 60 and 200 mgCu/L $CuSO_4$. Control cultures were not supplemented with $CuSO_4$. Cell growth was monitored by culture OD_{600nm}.

The effect of $CuSO_4$ in the formation of colony forming units (CFU) was also studied for cultures exposed to 40 and 60 mgCu/L $CuSO_4$, for 24h (Figure 4.3). The cultures exposed to 40 mgCu/L $CuSO_4$ took more time to increase the CFU concentration on the first 10h of exposure, compared with control, but it is possible to verify that the CFU concentration, after 24 h exposure, achieved the same CFU concentration as the control cultures (Figure 4.3). The CFU of cultures exposed to 60 mgCu/L $CuSO_4$, showed a similar behaviour up to 8 h exposure. However after 24h the number of CFU decrease abruptly (Figure 4.3).

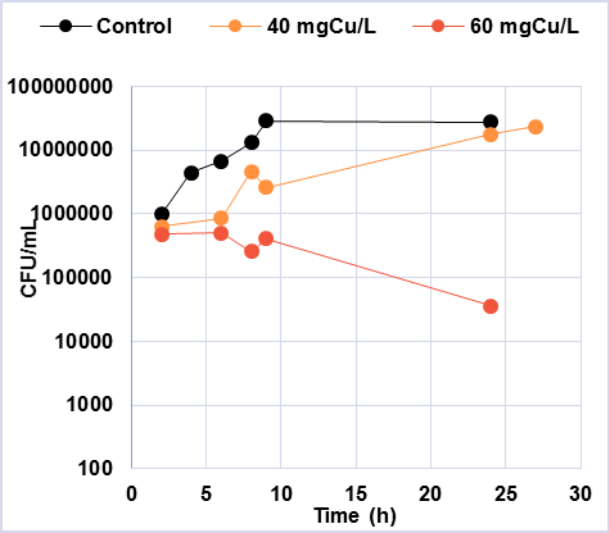

Figure 4.3 Colony unit formation of *Saccharomyces cerevisiae* BY4741 in a MM4 liquid medium (pH 4.5) supplemented with different concentrations of $CuSO_4$. Yeast viable cells in cultures supplemented with 40 and 60 mgCu/L $CuSO_4$. Control cultures were not supplemented with $CuSO_4$. The concentration of viable cells was assessed by colony forming units per millilitre of cell culture (CFU/mL).

The effect of $CuSO_4$ in the single gene deletion mutant, *S. cerevisiae* BY4741_Δ*cup2*, was also evaluated. The mutated gene, CUP2, is a copper-binding transcription factor that activates the transcription of a metallothionein encoding gene in response to high copper concentrations[47,48].

In Figure 4.4 are presented the growth curves of *cup2Δ* cultures exposed to increasing concentrations (6, 10, 20, 40 and 60 mgCu/L) of $CuSO_4$. As for wild-type cultures, the cell growth was followed by measuring the OD_{600}nm, over 28 h incubation. The results show that all the cultures exposed to $CuSO_4$ slightly increase, suggesting a growth inhibition of at least 28 h incubation (Figure 4.4). These results confirm the higher susceptibility of the *cup2Δ* to $CuSO_4$ (Figure 4.4), when compared with the wild-type (Figure 4.2).

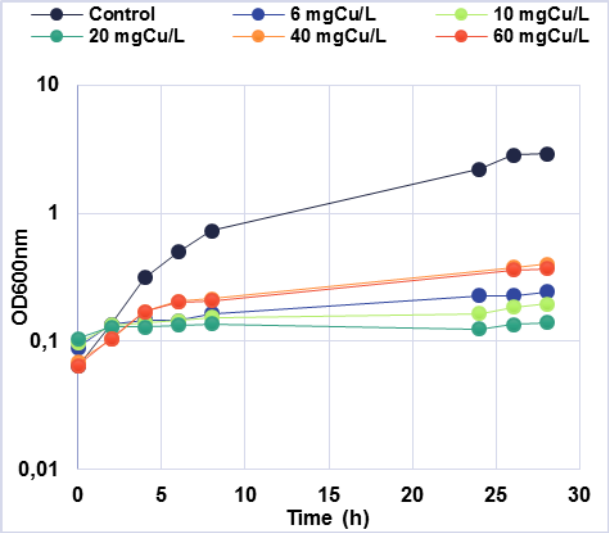

Figure 4.4 Growth curves of *Saccharomyces cerevisiae* BY4741_*Δcup2* in a MM4 liquid medium (pH 4.5) supplemented with different concentrations of $CuSO_4$.
Growth curves cultures supplemented with 6, 10, 20, 40 and 60 mgCu/L $CuSO_4$ Control cultures were not supplemented with $CuSO_4$. Cell growth was monitored by culture OD_{600nm}.

The effect of $CuSO_4$ in the formation of CFU was also evaluated for *cup2Δ* cultures, exposed to 6, 10, 20, 40 and 60 mgCu/L $CuSO_4$. The assay was performed for 26h and the results can be depicted in Figure 4.5.For exposure conditions with Cu concentrations up to 20 mgCu/L, the CFU concentrations remained nearly constant over the incubation time (Figure 4.5). The CFU formation in cultures exposed to 40 and 60 mgCu/L $CuSO_4$ drastically decreased after 8h, reaching CFU concentrations 10,000 times lower than the controls (Figure 4.5).

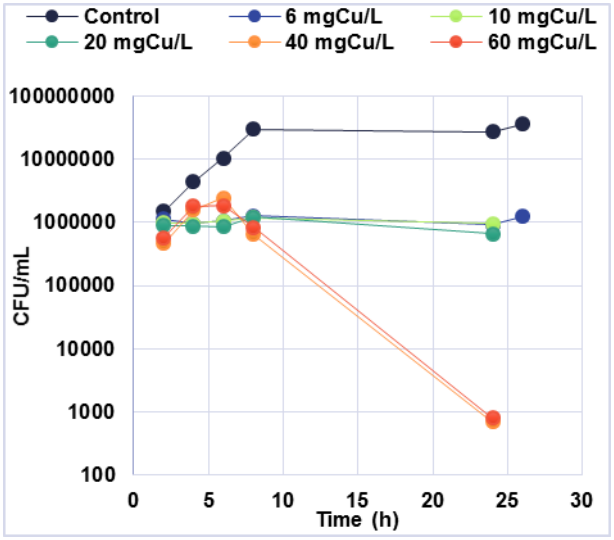

Figure 4.5 Colony unit formation of *Saccharomyces cerevisiae* BY4741_*Δcup2* in a MM4 liquid medium (pH 4.5) supplemented with different concentrations of $CuSO_4$.
Yeast viable cells in cultures supplemented with 6, 10, 20, 40 and 60 mgCu/L $CuSO_4$. Control were no supplemented c. Control cultures were not supplemented with $CuSO_4$. The concentration of viable cells was assessed by colony forming units per millilitre of cell culture (CFU/mL).

The CFU assays demonstrated a higher susceptibility of the *cup2Δ* mutant for $CuSO_4$ when compared with the results obtained for the wild-type cultures. Specifically, cultures exposure to 40 mgCu/L of $CuSO_4$, yielded different outcomes. The wild type cultures (Figure 4.3) even showing a slow growth increase were able to increase the CFU over incubation time, whereas the *cup2Δ* mutant displayed a drastic CFU decrease for the same concentration, (Figure 4.5).

4.2.2 The effect of CuO-NPs in *Saccharomyces cerevisiae* strains growth

The effect of CuO-NPs in *Saccharomyces cerevisiae* BY4741 cultures was examined using growth conditions as described in section 3.2. As in the assay with $CuSO_4$, the growth of *S. cerevisiae* BY4741 in the presence of CuO-NPs was followed by measuring OD_{600nm} over 30 h incubation (Figure 4.6) and compared to cultures without NPs supplementation (control conditions). A range of CuO-NPs concentrations from 6-100 mgCu/L were tested. The results obtained are summarized in Figure 4.6.

Although the preliminary results on the effect of CuO-NPs in yeast cell growth attained to indicate a decrease on the specific growth rate and a reduction of the final biomass in cell cultures, the effect of exposure to CuO-NPs cannot be assessed by measuring the culture OD_{600nm} due to the interference of the CuO-NPs with the this measurement. The concentration of viable cells was then assessed instead by using the colony forming unit (CFU) technique.

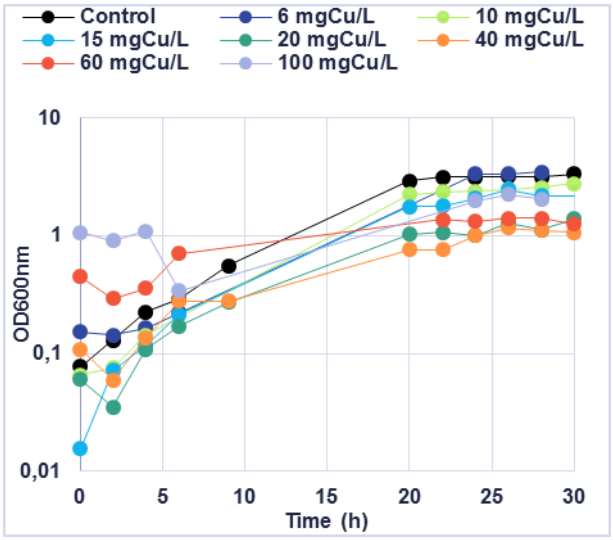

Figure 4.6 Growth curves of *Saccharomyces cerevisiae* BY4741 in a MM4 liquid medium (pH 4.5) supplemented with different concentrations of CuO-NPs. Growth curves of cultures supplemented with 6, 10, 15, 20, 40, 60 and 100 mgCu/L equivalent in CuO-NPs. Control cultures were not supplemented with CuO-NPs. Cell growth was monitored by culture OD_{600nm}.

The concentration of viable cell from cultures exposed to concentrations of CuP-NPs equivalent to 10 mgCu/L to 40 mgCu/L were assessed by the CFU assay for 30 h (Figure 4.7).

The growth curves represented above (see Figure 4.6) showed a growth rate increase up to 8 h incubation for control and CuO-NPs exposed cultures alike. However, when assessing CFU concentrations, the cell cultures exposed to CuO-NPs concentrations higher than 15 mgCu/L showed a decrease in viable cells up to 28h, while cultures cultivated with CuO-NPs ≤ 15 mgCu/L showed an increase of the concentrations of viable cells similar to the increase registered in the control culture (Figure 4.7).

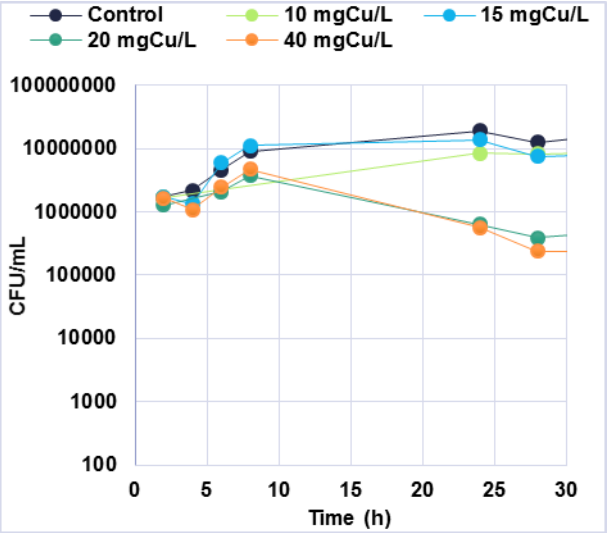

Figure 4.7 Colony unit formation of *Saccharomyces cerevisiae* BY4741 in a MM4 liquid medium (pH 4.5) supplemented with different concentrations of CuO-NPs.
Yeast viable cells in cultures supplemented with 10, 15, 20 and 40 mgCu/L CuO-NPs. Control cultures were not supplemented with CuO-NPs. The concentration of viable cells was assessed by colony forming units per millilitre of cell culture (CFU/mL).

The susceptibility of the *cup2Δ* mutant to CuO-NPs was also examined. The Figure 4.8 displays the growth curves of *cup2Δ* cultures exposed to increasing concentrations (6, 10, 15 and 40 mgCu/L) of CuO-NPs. As in previous assays the cell growth was followed by measuring the OD_{600nm}, over 28 h incubation. For the first 8 h of incubation with CuO-NPs, cell cultures did not display cell growth, contrasting with controls. However, an increase in cell growth after 24h of incubation was observed in cultures exposed to concentrations higher than 15 mgCu/L (Figure 4.8). This was likely related to the CuO-NPs interference with the OD_{600nm} measurement.

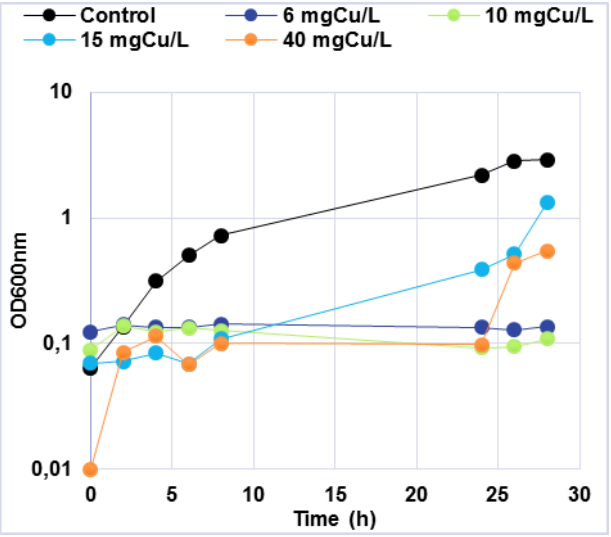

Figure 4.8 Growth curves of *Saccharomyces cerevisiae* BY4741_*Δcup2* in a MM4 liquid medium (pH 4.5) supplemented with different concentrations of CuO-NPs.
Growth curves cultures supplemented with 6, 10, 15, and 40 mgCu/L CuO-NPs. Control cultures were not supplemented with CuO-NPs. Cell growth was monitored by culture OD_{600nm}.

In fact, the CFU assay showed a different picture. The analysis of the CFU numbers in cultures exposed to CuO-NPs, showed that the CFU concentrations decreased with incubation time for all the concentrations examined. Also, the decrease of CFU concentration was CuO-NPs concentration dependent (Figure 4.9).

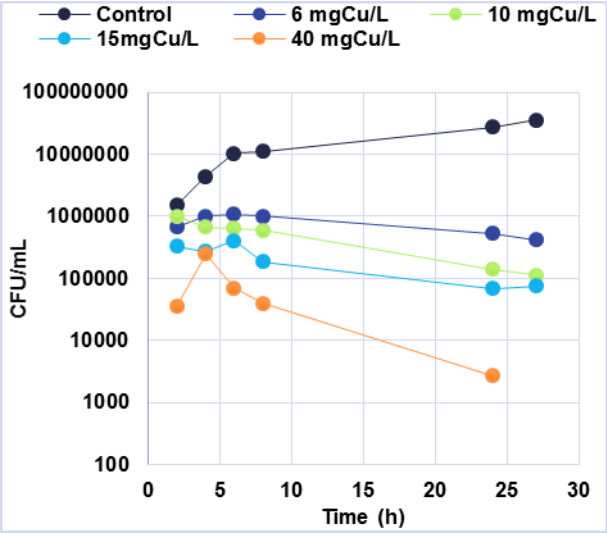

Figure 4.9 Colony unit formation of *Saccharomyces cerevisiae* BY4741_*Δcup2* in a MM4 liquid medium (pH 4.5) supplemented with different concentrations of CuO-NPs.
Yeast viable cells in cultures supplemented with 6, 10, 15 and 40 mgCu/L CuO-NPs. Control cultures were not supplemented with CuO-NPs. The concentration of viable cells was assessed by colony forming units per millilitre of cell culture (CFU/mL).

4.2.3 Differences between the effect of CuO-NPs and $CuSO_4$ in *Saccharomyces cerevisiae* strains growth

Results obtained with the wild-type cultures indicated to be more susceptible to the presence of CuO-NPs than equivalent Cu concentrations as $CuSO_4$. Whereas yeast cell cultures were most affected by exposures of 40 mgCu/L $CuSO_4$ (see Figure 4.3) when exposed to the equivalent Cu concentration of CuO-NPs a sharp decrease of the concentration of viable cells after 8h incubation was observed (Figure 4.7). Furthermore, this pattern was displayed for Cu concentration levels as low as 20 mgCu/L CuO-NPs (Figure 4.7).

The results obtained with *cup2Δ* mutant strain indicated higher susceptibility for both CuO-NPs and $CuSO_4$. Cell cultures exposed either to CuO-NPs (Figure 4.9) or $CuSO_4$ (Figure 4.5), displayed similar CFU concentrations for equivalent concentrations of copper.

4.3 Effect of CuO-NPs in the level of protein oxidation in *S. cerevisiae* strains

The effect of CuO-NPs in the level of protein oxidation was assessed to inspect possible mechanisms of interaction of CuO-NPs with cells that may justify the detrimental outcomes observed on yeast growth. As described in Section 3.4 the sulfydryl-reactive agent maleimide–PEG2– biotin (MPB) was used to assess the reduction of thiolate anions in proteins as a measure of corresponding oxidative damage.

The yeast strains exposed to CuO-NPs were studied against control cultures (non-supplemented) and positive controls supplemented with equivalent concentrations of Cu ($CuSO_4$). The results obtained for the presence of protein thiol groups were similar in both *S. cerevisiae* cells, wild-type and *cup2Δ*. Cell extracts harvested after 6 h of exposure to both CuO-NPs and $CuSO_4$ Cu-equivalent concentration of 40 mgCu/L, showed almost undetectable MPB labeling (Figure 4.10).

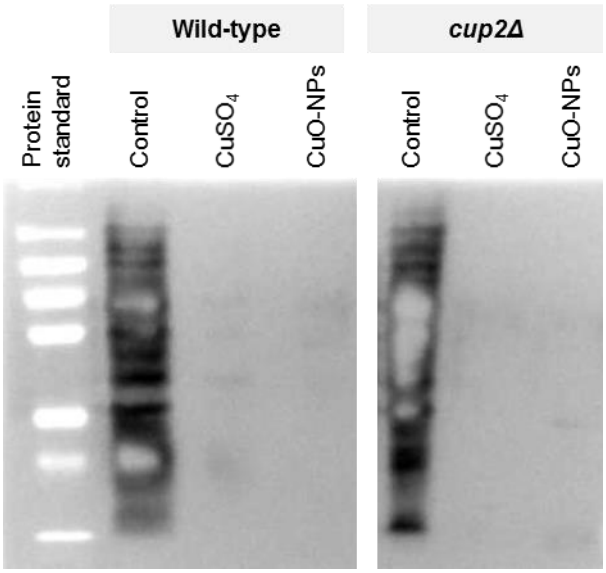

Figure 4.10 Immunodetection of maleimide reactive molecules expressing protein thiol reactive groups in *S. cerevisiae* wild type and cup2Δ exposed to CuO-NPs and $CuSO_4$. Labeled protein extracts were obtained from wild-type cells and *cup2Δ* cells after cultivation for 6 h, exposure to 40 mgCu/L of $CuSO_4$ and 40 mgCu/L CuO-NPs. Controls were obtained from no supplemented cells. The white spots visible in the controls are due to the formation of air bubbles in the sample.

This result strongly suggests that both copper solution and NP suspensions at the concentration examined induced large cysteine oxidation, either in wild-type or in *cup2Δ* cells.

However, the assay should be repeated with a lower concentration of $CuSO_4$ and CuO-NPs, and with varying exposure times (lower than 6h) in order to improve the differentiation of protein oxidation levels between wild-type and mutant cultures under the different chemical compound.

4.4 Copper quantification in *Saccharomyces cerevisiae* cells

Individual *S. cerevisiae* cells (wild-type and *cup2Δ*) were analysed with nuclear microscopy, in order to identify differences in cellular Cu distribution. The studied conditions were cell cultures exposed to CuO-NPs and $CuSO_4$. Typical images of Cu distribution in *S. cerevisiae* cells can be depicted in Figure 4.11. The distribution maps of K, a physiological important element in yeast physiology, in relationally higher concentrations, are also represented to help defining the cell boundaries.

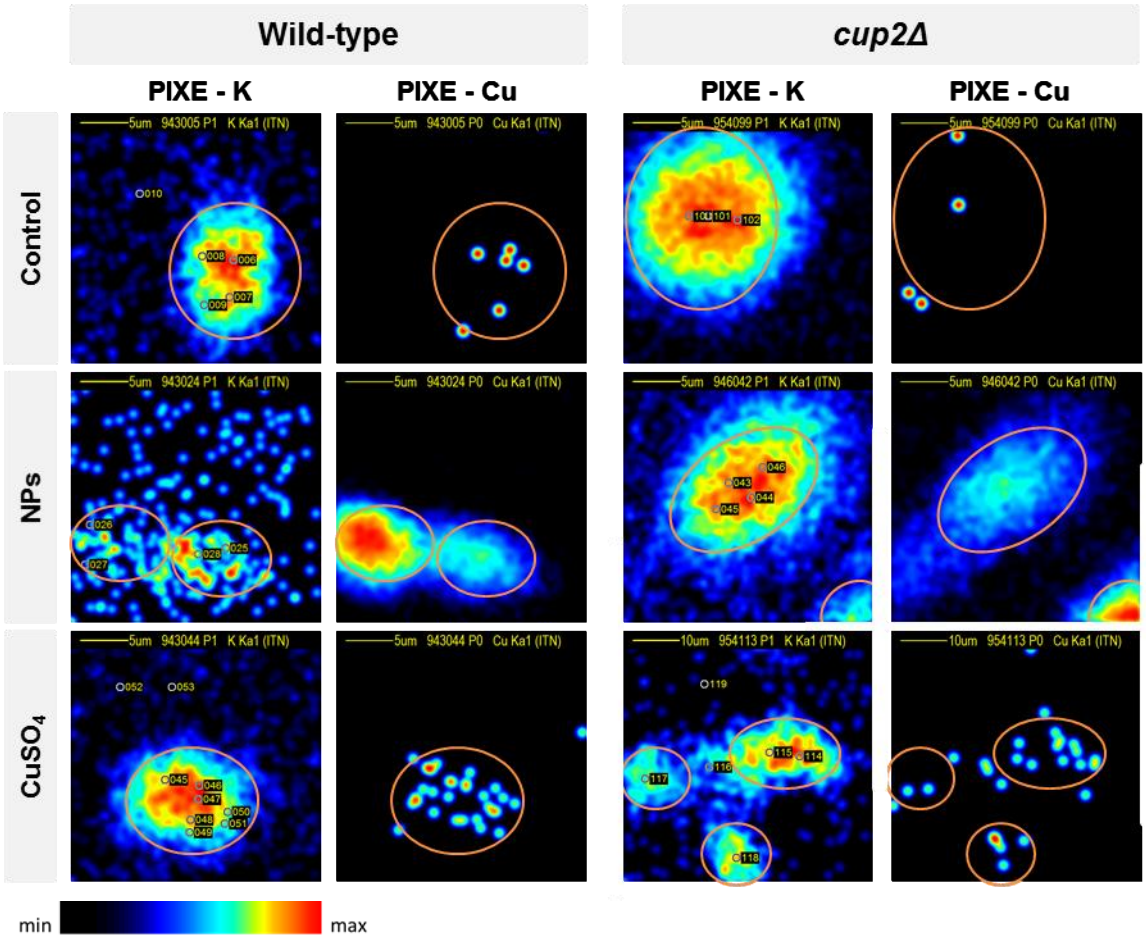

Figure 4.11 Nuclear Microscopy images of *S. cerevisiae* wild-type and *cup2Δ* cells.
Images of K and Cu, from *S. cerevisiae* wild-type cells and *cup2Δ* cells are displayed. Top panel: without Cu supplementation – Control; Middle panel: exposed to 40mgCu/L CuO-NPs; Low panel: exposed to 40mgCu/L $CuSO_4$. The images were obtained with PIXE technique using protons at 2.0 MeV as projectile. The dots displayed in the K maps indicated the regions used for the quantitative elemental determination.

The images of cells of both *S. cerevisiae* strains supplemented with CuO-NPs, showed significantly higher Cu levels than control cells (non-supplemented cells). Comparing the Cu distribution maps, it can also be inferred that the cells exposed to CuO-NPs accumulated more Cu than cells exposed to the equivalent Cu concentration delivered by $CuSO_4$.

The concentrations of Cu in yeast cells were determined using, simultaneously, PIXE and RBS techniques, as described previously (see Methods 3.5). The Cu concentrations in *Saccharomyces cerevisiae* BY4741 cells, non-exposed (control), and exposed to CuO-NPs (15, 20 and 40 mgCu/L) and to $CuSO_4$ (40, 60 mgCu/L) were determined the concentrations were measured in samples taken after 6h and 24h of incubation. The Cu concentrations of cell cultures exposed to CuO-NPs were compared to controls and cells exposed to $CuSO_4$ in equivalent levels of Cu concentration (See (Figure 4.12 A and B). Higher Cu concentrations in cells exposed to NPs (Figure 4.12, panel B) were observed by report to non-supplemented cells and supplemented with equivalent concentrations of $CuSO_4$ (Figure 4.12, panel A).

The cells exposed to 40 mgCu/L CuO-NPs have 200 times more Cu, than the cells exposed to $CuSO_4$. It is also possible to infer that in cells exposed to CuO-NPs, the Cu concentration in cells increased as a function of exposure concentration. This is not observable in cells exposed to $CuSO_4$, where the Cu concentration in cells exposed to 40 mgCu/L and 60 mgCu/L of $CuSO_4$ did not significantly change.

The Cu concentration in cells exposed to CuO-NPs decreased with exposure time, i.e., the Cu concentration in cells diminished after 24 h of exposure when compared to cells exposed for 6h to the same Cu concentration. This may indicate loss of cell integrity, as viability studies described previously suggested.

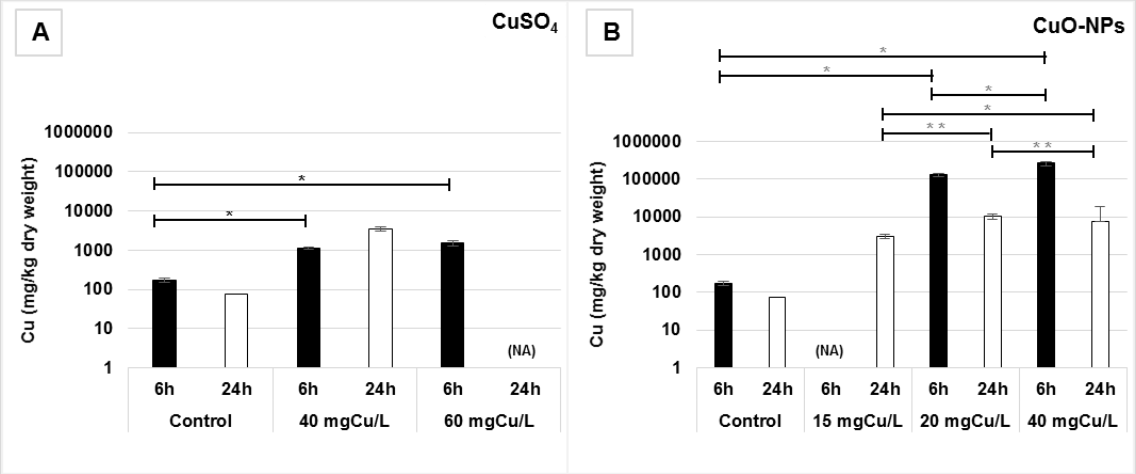

Figure 4.12 Concentration of copper in *Saccharomyces cerevisiae* BY4741 cells cultured in MM4 liquid medium supplemented with $CuSO_4$ and CuO-NPs.
The *S. cerevisiae* BY4741 cells were collected after 6 h of growth and after 24 h of growth in the presence of 40 and 60 mgCu/L of $CuSO_4$ (panel A) or 15, 20 and 40 mgCu/L of CuO-NPs (panel B). No supplemented cultures served as control. Asterisks indicate significant differences for $p < 0.05$ (*) and $p < 0.01$ (**).Some conditions were not analysed (NA).

Examining the Cu concentrations in *S. cerevisiae* BY4741_Δ*cup2* mutant cells, exposed to both CuSO4 and CuO-NPs, similar results to those observed in wild-type cells were obtained (Figure 4.13). The Cu concentration, in Δ*cup2* cells exposed to CuO-NPs was 250 times higher than in cells expose to $CuSO_4$. Also, the increase of Cu concentration in cells was dependent on CuO-NPs exposure levels.

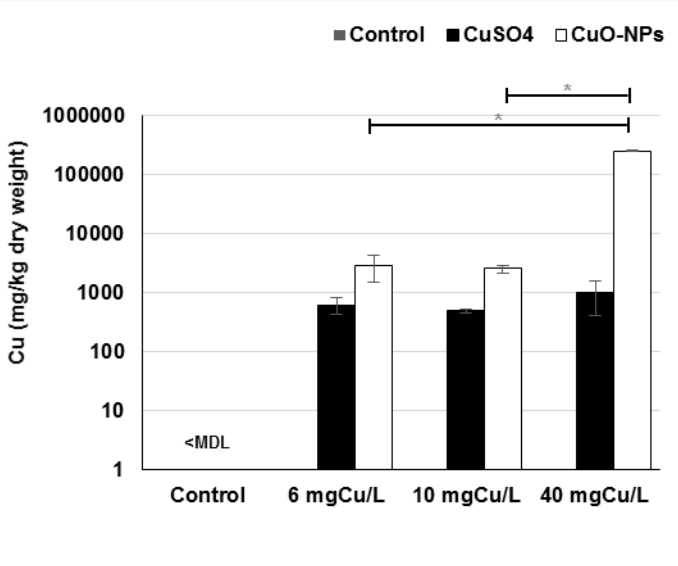

Figure 4.13 Concentration of copper in *S. cerevisiae* BY4741_ *Δcup2* cells growing in MM4 liquid medium and supplemented with CuO-NPs.
The *S. cerevisiae* BY4741_*Δcup2* cells were collected after 6 h of growth in the presence of 6, 10 and 40 mgCu/L of CuO-NPs or $CuSO_4$. No supplemented cultures served as controls. Values below the minimum detection limit are represented by <MDL. Asterisks indicate significant differences for $p < 0.05$.

However, the images obtained for the Cu distribution in cells and the quantitative measures of Cu in cells cannot assure whether Cu was uptake by cells or is deposited on the cell surface The Cu images displayed in Figure 4.11 and the Cu concentrations determined were obtained from PIXE spectral data, which integrates X-rays originated from all sample depths. To inspect at which distance from cell surface Cu can be found, a technique with depth resolution capabilities has to be applied.

4.5 CuO-NPs accumulation in *Saccharomyces cerevisiae* strains

In order to investigate if the CuO-NPs or Cu-derived from NPs were internalized by *S. cerevisiae*, the capability of Rutherford Backscattering Spectrometry (RBS) depth profiling was explored. The backscattered energy of the projectile is dependent on its path in and out the sample and also on the mass of the atomic nuclei to which it collides. Therefore, RBS data can give the depth, in the sample matrix, where the atom causing the beam scattering is. Also the energy of the backscattered particles can also be expressed in terms of thickness. This concept is illustrated using a region of the typical RBS spectra corresponding to Cu in Figure 4.14. The region can be analysed for slices of energy, which correspond to a certain sample depth. In the case of a single cell, the total energy interval corresponding to the cell thickness of 1 μm was considered.

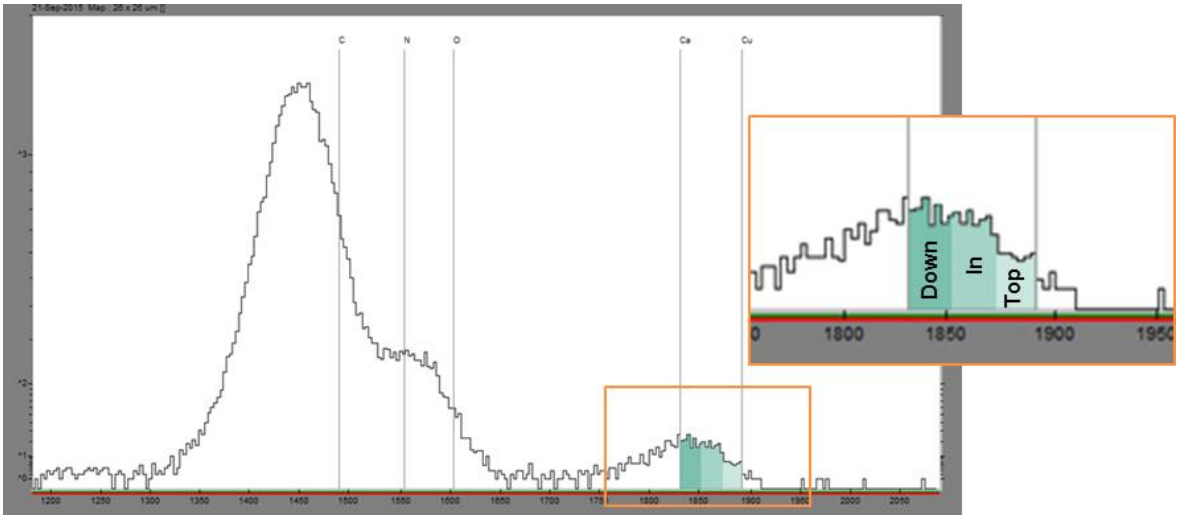

Figure 4.14 Typical RBS spectrum of *S. cerevisiae* cells exposed to CuO-NPs, illustrating the methodology used and the depth resolution estimation based on the cell matrix.
Spectrum from the analysis of *S. cerevisiae* cells exposed to CuO-NPs. The spectrum were obtain through RBS technique using protons at 2.0 MeV as projectile. The amplified image illustrate the three sections analysed in order to inquire the location of the CuO-NPs in the cells. The colour of the sections it gets darker with the depth of the cell.

This interval of energies allowed examining most yeast cells along its entire depth without contribution from other elements, such as Ca and K for instance because these elements are representative in biological cells.

The thickness interval corresponding to the backscattered energies between Ca and Cu (Figure 4.14) was used for selecting different layers of the cell (Figure 4.15). The thickness of each layer was estimated having into account the interval of energy variation that can be resolved by the detector. This was done by incrementing depth at which Cu could be found in ~50nm steps and measuring backscattered energy of the protons. The depth of each slice corresponding to the energy interval that can be discriminated was found to be of the order of 150-200 nm for protons (the projectile used).

The information contained in each slice of energy extracted from RBS data can be plotted and the Cu distribution visualized. The images of the three layers describing the cell in its depth can be depicted in Figure 4.15. The Cu localization on top regions of the cell within a thickness that is of the order of *S. cerevisiae* wall[61] and inside the cell (Figure 4.15) can then be estimated. The deepest layer (down in Figure 4.15) may have the contribution of both backing where the cell is attached and the cell wall.

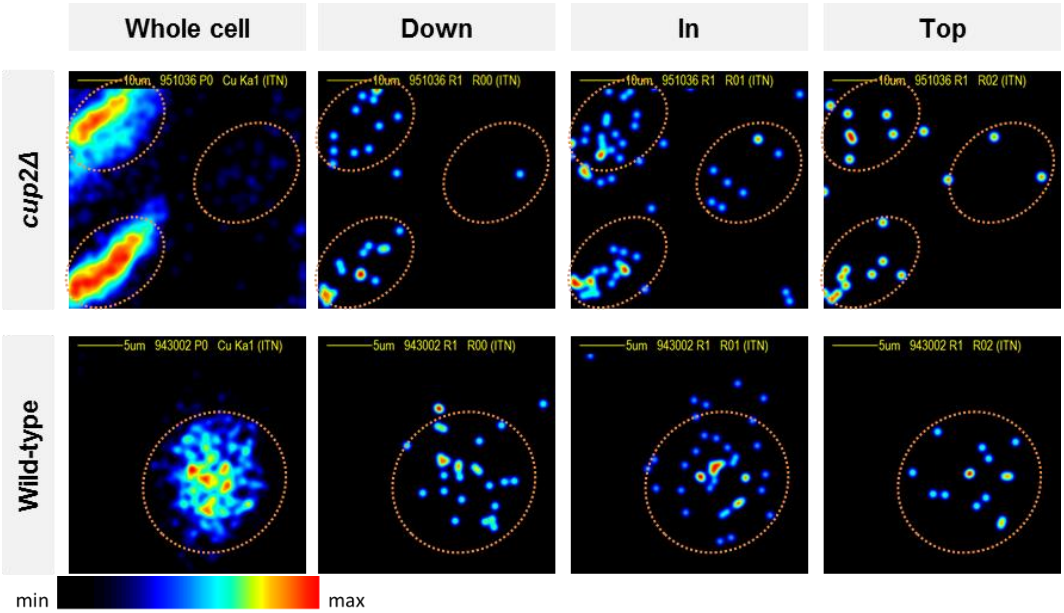

Figure 4.15 Imaging the Cu in *S. cerevisiae* WT and Δ*cup2* cells, and the Cu in different sections of the cell.
The images were obtained through RBS technique using protons at 2.0 MeV as projectile. Images of the copper content in *S. cerevisiae* cell after the exposure to CuO-NPs. The wild-type cells were expose to 20 mgCu/L CuO-NPs and the mutant cells (*cup2Δ*) were expose to 15 mgCu/L CuO-NPs. The images on the left display de image from the whole cell analysis. The three images from de right display the images obtained from different sections of the cell (top, in and down).

The images obtained showed that in both *S. cerevisiae* strains exposed to CuO-NPs, Cu was found inside the cells. The Cu signal appeared to be higher inside the cell (Figure 4.15, “In”), relative to top layer (”Top”), which mainly corresponds to cell wall. The amount of Cu in the bottom layer (Figure 4.15, “Down”) seems to be similar to the medium layer “In” and higher than the content on the cell surface (Figure 4.15, “Top”). This could be explained by the fact that this layer may contain information of both internal cell media, cell wall and cell backing as referred above. Cells are attached to the polycarbonate foil (backing), which may retain CuO-NPs present in the culture media. Other possibility for Cu signal increment may derive of cell geometry changes. Attached cells on the foil may lose their typical spherical morphology, which may lead to a compression of cellular contents. It is not noticeable an increase in the copper content in the limits of the cells indicating that the CuO-NPs do not preferentially aggregate to cell wall. Instead, Cu was found to spread through the intracellular space. Therefore, the distribution images of Cu along cell depth unequivocally showed that Cu derived from CuO-NPs was internalized.

5 Discussion

In this study we examined the toxic effect of copper oxide NPs (CuO-NPs) in the yeast *Saccharomyces* cerevisiae as a toxicity model. It was used both the parental *Saccharomyces cerevisiae* BY4741 (wild-type) and the derived single deletion mutant BY4741_*Δcup2* (*cup2Δ*), where the CUP2 gene was deleted. This gene encodes a transcription factor which induce the CUP1 and CRS5 genes, associated to copper detoxification mechanisms by the biosynthesis of metallothioneins. Both strains were exposed to different concentrations of CuO-NPs having as reference yeast cells which were exposed to equivalent concentrations of $CuSO_4$ and non-exposed cells as control. The most notable results obtained in this study were: i) yeast cells accumulate and internalize more copper when exposed to CuO-NPs than when they are exposed to equivalent concentrations of $CuSO_4$; and ii) CuO-NPs shares the cellular mechanisms used in Cu^{2+}/Cu^{+} detoxification.

We initially studied the effect of $CuSO_4$ in *Saccharomyces cerevisiae* with the aim to estimate inhibitory Cu concentration levels in yeast growth, for subsequent tests with CuO-NPs. The results obtained show that cultures exposed to $CuSO_4$, with concentrations up to 200 mgCu/L, for 24h exhibit a dose-dependent progressive growth delay until growth was fully inhibited at 200 mgCu/L. These concentration levels of $CuSO_4$ and incubation period of time up to 30h were reported to inhibit growth of *S. cerevisiae* [62]. However, cell viability decreased 40 mgCu/L, as indicated by CFU determination assays. The effect of $CuSO_4$ was also tested on a single gene deletion mutant, *S. cerevisiae* BY4741_*Δcup2* (*cup2Δ*). Our results show that the mutant *cup2Δ* exhibits a higher susceptibility to $CuSO_4$ compared to the wild-type. This result was expected since *cup2Δ* has the CUP2 gene deleted and this gene encodes a copper-binding transcription factor that activates the transcription of metallothionein gene (CUP1 and CRS5) in response to growth inhibitory copper concentrations[47,48]

The proteins with antioxidant properties play an important role in Cu sequestration[63,64]. Yeast metallothionein encoded by *CUP1* detoxifies Cu ions by tightly sequestering seven atoms of Cu(I) through coordination with the thiolate ligands of the abundant cysteine residues in the protein[65]. In the absence of CUP2 gene, this mechanism is hampered.

The evaluation of growth in cultures exposed to CuO-NPs could not be followed by OD_{600nm} measurement due to CuO-NPs interference. This was circumvented by studying the number of CFU. The assays of the determination of CFU, for wild-type and *cup2Δ* cultures, indicated that wild-type cultures were more susceptible do CuO-NPs than to $CuSO_4$, showing a significant decrease of cellular viability at 20 mg/L and 60 mg/L, respectively. In addition, our results showed similar CFU concentrations in *cup2Δ* cultures exposed to CuO-NPs and $CuSO_4$, indicating similar susceptibility of *cup2Δ* for both copper compounds. This contrasted with the results obtained for the wild-type cultures, where a higher susceptibility was observed for cultures exposed to CuO-NPs than those exposed to equivalent concentrations of $CuSO_4$.

The toxicity of CuO-NPs towards *S. cerevisiae* is still not consensual. Bayat et al. [66] had demonstrated the cyto- and genotoxicity of CuO-NPs. Kasemets et al[9] had shown that both nano- and bulk CuO was toxic to *S. cerevisiae*. However, opposite to our results, the CuO-NPs were reported to be less toxic than $CuSO_4$ (Kasemets et al[9]). In fact the results are not totally comparable, as experimental conditions greatly differ. Kasemets et al[9] used different growth media (YPD) and incubation conditions (microplate incubation for 24h without agitation). The CuO-NPs aggregation study performed in our study demonstrated that aggregation has to be considered relevant after 8h of incubation.

Kasemets et al.[9] also studied mutant strains of *S. cerevisiae*, demonstrating that the single deletion mutant *cup2Δ* is more susceptible to CuO-NPs than wild-type. These results corroborate our findings, as they indicated that the detoxification mechanisms activated by CUP2 gene (absent in the mutant) is also acting in the detoxification of CuO-NPs.

Studies with several single mutants associated with oxidative stress defences and susceptibility suggested that CuO-NPs toxicity was associated to different oxidative stress mechanisms than menadione and H_2O_2 (Kasemets et al[9]). Our study, the determination of protein free thiol groups, show that both $CuSO_4$ and CuO-NPs induce massive oxidation of the cysteines of cellular proteins in both strains (wild-type and *cup2Δ*). These results indicated that the used Cu concentrations affected the redox balance in yeast, through its action as a thiol compound. The *S. cerevisiae* Cup1 and Crs5 metallothioneins scavenge excess Cu by tight coordination with cysteine thiolates (Festa et al[47]). Therefore, the extensive protein oxidation observed in the *cup2Δ* mutant cultures after CuO-NPs exposure clearly related the metallothioneins detoxification mechanism of Cu derived from CuO-NPs. Our prospective study on protein oxidation levels could be tuned and improved by using lower CuO-NPs concentrations and smaller exposure incubation times, than those tested. This would definitely improve the sensitivity of the method and would provide more clear results of the yeast response to CuO-NPs.

The results obtained in this study strongly suggest that CuO-NPs can be transferred to the yeast intracellular environment. However, to assess intracellular Cu is challenging. The accumulation of Cu in cell cultures is traditionally achieved with reference analytical techniques, such as Inductively Coupled Plasma Mass Spectrometry (ICP-MS) and Atomic Absorption Spectrometry (AAS). These techniques can quantify the bulk Cu contents in cell pellets and culture medium with high sensitivity. They usually require strict sample preparation procedures besides adequate sample amount. Nevertheless, these techniques cannot provide data for the intracellular Cu content. In this study as an alternative, nuclear microscopy techniques were used for the Cu quantification in *S. cerevisiae* individual cells. This approach has been used for the qualitative and quantitative elemental analysis in numerous *in vitro* assays with cell cultures, including *S. cerevisiae* (Ohnuki et al[67], Kern et al[68], Ortega et al[69], Watt et al[70]). The combination of techniques used can deliver two-dimensional images of the Cu distribution in cells and quantitate Cu contents in whole individual cells. Moreover, the evaluation of Cu deposited on the cell surface and inside the cell can be determined.

Our results showed that Cu concentrations were similar in both wild-type and *cup2Δ* strains exposed to CuO-NPs. However, for equivalent Cu concentrations in the culture media, the Cu concentration was greater in yeast cells exposed to CuO-NPs than in those exposed to $CuSO_4$. Similar findings were found in the literature. Cronholm et al[71] reported on higher uptake of CuO-NPs compared to nil or low uptake of the soluble salts. The higher Cu concentration in cells exposed to CuO-NPs cannot be only associated to cellular detoxification mechanisms, since, as previously mentioned, Cu distribution was similar in both strains. Bondarenko et al[3] suggested a CuO-NPs uptake by endocytose (Trojan horse model) in mammalian cells. These authors also hypothesized that when inside the cell, CuO-NPs may solubilize obstructing the regulator mechanisms for Cu ions in the cell (e.g., detoxification mechanisms) hindering their normal function. Yet, the mechanism by which CuO-NPs can enter in the yeast cell is unknown.

We also observed that Cu concentration in cells exposed to CuO-NPs diminished after 24 h of exposure. This could be justified by oxidative damage caused by CuO-NPs to membrane proteins thiols, hypothetically through similar mechanisms as those assessed in our study. Oxidative damage to lipids may also occur[7,9]. All together, these events may lead to increased membrane permeability or even cell lysis, enabling the leakage of intracellular constituents, such as Cu previously captured. Avery et al.[63] demonstrated the exposure of *S. cerevisiae* to elevated Cu^{2+} concentrations was associated with a rapid (within minutes) permeabilization of the *S. cerevisiae* plasma membrane. The toxicity of CuO-NPs was proposed to cause damage in cellular membrane. Karlsson et al.[7] have studied the effect of the CuO-NPs in biological membranes demonstrating that CuO-NPs can interact by adsorbing on the phospholipid membrane surface, giving rise to alterations on its viscoelastic properties. The CuO-NPs addition changed the phospholipid assembly causing an increase of dissipative losses. These findings could explain the viability loss and the decrease of Cu content observed in yeast cultures exposed to CuO-NPs after 24h of exposure.

In this work images of the Cu distribution in whole cells and Cu depth profiles were established. By using the depth analysis capabilities of RBS technique it was possible to demonstrate for the first time the internalization of Cu derived from CuO-NPs in *S. cerevisiae* cells, of both strains (wild-type and *cup2Δ*). These results proved that nuclear microprobe techniques and especially RBS depth analysis are unique tools to determine whether NPs are internalized by cells and also to establish where NPs are accumulating inside cells. However, the experimental conditions used in our work only enabled depth resolutions of the order of 200 nm, which limited detailed evaluation of Cu distribution inside the cell. The use of different beams (heavier projectiles) and different incident energies it will be possible to enhance the cell depth discrimination below 80 nm resolution for Cu. This will be of the utmost relevance for 3D reconstruction of cells that will allow imaging NPs location in cells. 3D structural identification of NPs in HeLa cells were already accomplish by Chen et al[58].

One crucial issue in studies with NPs is the stability of the nanomaterial in biological media [72] .In this study only a superficial characterization of the physical properties of CuO-NPs was carried

out to assure the size distribution of CuO-NPs during experiments. The agglomeration indexes calculated, showed that the CuO-NPs size distribution remains stable through the time of the exposure tests. However the CuO-NPs distribution broadened, indicating an increase of average distribution of particle sizes, after 24 hours. Bayat et al[66] also demonstrated that the CuO-NPs had larger hydrodynamic sizes in exposure medium, advising for potential aggregation and/or agglomeration of the CuO-NPs, when not in deionised water. In order to a better characterization of the CuO-NPs, several methods such as ultramicroscopy imaging, size exclusion chromatography and scattering techniques can be used for submicron particle size analysis. Among these, electronic microscopy analysis (such as TEM and SEM) provides direct estimate of size, shape and texture in high resolution. As a future work the use of different techniques for the characterization of the CuO-NPs would be interesting for a better understanding of the relation between the its physico-chemical properties and its toxicological effect.

6 Conclusions and future perspectives

This study highlighted the potential of *S. cerevisiae* as a model to study nanoparticles toxicity and the adequacy of screening methodologies developed. The study enabled to visualize and quantify Cu distribution in whole cells and for the first time, across their depth. It was demonstrated that yeast cells accumulated CuO-NPs and that protein oxidative damage was likely caused by Cu derived from CuO-NPs internalized in the cell.

"How the CuO-NPs enter the cell?" and which metabolic pathways are affected by the CuO-NPs?" are two of the biggest questions that remains unidentified. The answers for these questions may be achieved by the use of mutants associated to different transporters and metabolic pathways, for a better understanding of the uptake mechanisms used and of the response of the cell for these NPs. We have realised that CuO-NPs had an effect on protein oxidation, however, it would be enlightening in the yeast response to CuO-NPs, if the assay was conducted in different experimental conditions (lower CuO-NPs concentrations and smaller exposure incubation times). Nuclear microscopy revealed to be a useful technique for the visualization/quantification of NPs in cells. Nevertheless the potential of this technique can be further explored with the use of different beams and projectile energies, to eventually achieving a 3D identification of the NPs in cell, helping the understanding at which structural level the NPs act in the cell. In order to achieve an improved comprehension of the CuO-NPs effect in cells, a deeper study of the CuO-NPs physical characteristics is proposed. The use of different characterization techniques can help in achieving that purpose.

The preliminary results obtained encourage further studies using selected mutants to deepen scientific knowledge on mechanisms and modes of action of CuO-NPs.

7 References

1. Murdock, R. C., Braydich-Stolle, L., Schrand, A. M., Schlager, J. J. & Hussain, S. M. Characterization of nanomaterial dispersion in solution prior to in vitro exposure using dynamic light scattering technique. *Toxicol. Sci.* **101,** 239–253 (2008).

2. Kasemets, K., Ivask, A., Dubourguier, H. & Kahru, A. Toxicology in Vitro Toxicity of nanoparticles of ZnO , CuO and TiO 2 to yeast Saccharomyces cerevisiae. *Toxicol. Vitr.* **23,** 1116–1122 (2009).

3. Bondarenko, O. *et al.* Toxicity of Ag, CuO and ZnO nanoparticles to selected environmentally relevant test organisms and mammalian cells in vitro: A critical review. *Arch. Toxicol.* **87,** 1181–1200 (2013).

4. Vance, M. E., Kuiken, T., Vejerano, E. P., McGinnis, S. P., Hochella, M. F., Rejeski, D., Hull, M. S. Nanotechnology in the real world: Redeveloping the nanomaterial consumer products inventory. *Beilstein J. Nanotechnol.* **6,** 1769–1780 (2015).

5. Treuel, L., Jiang, X. & Nienhaus, G. U. New views on cellular uptake and trafficking of manufactured nanoparticles. *J. R. Soc.* (2013).

6. Käkinen, A., Bondarenko, O., Ivask, A. & Kahru, A. The Effect of Composition of Different Ecotoxicological Test Media on Free and Bioavailable Copper from CuSO4 and CuO Nanoparticles: Comparative Evidence from a Cu-Selective Electrode and a Cu-Biosensor. *Sensors* **11,** 10502–10521 (2011).

7. Karlsson, H. L., Cronholm, P., Hedberg, Y., Tornberg, M., De Battice, L., Svedhem, S., Wallinder, I. O. Cell membrane damage and protein interaction induced by copper containing nanoparticles-Importance of the metal release process. *Toxicology* **313,** 59–69 (2013).

8. Piret, J. *et al.* Copper(II) oxide nanoparticles penetrate into HepG2 cells, exert cytotoxicity via oxidative stress and induce pro-inflammatory response. *Nanoscale* **4,** 7168–7184 (2012).

9. Kasemets, K., Suppi, S., Künnis-Beres, K. & Kahru, A. Toxicity of CuO nanoparticles to yeast saccharomyces cerevisiae BY4741 wild-type and its nine isogenic single-gene deletion mutants. *Chem. Res. Toxicol.* **26,** 356–367 (2013).

10. Hosiner, D., Gerber, S., Lichtenberg-Fraté, H., Glaser, W., Schu, C., Klipp, E. Impact of Acute Metal Stress in Saccharomyces cerevisiae. *PLoS One* **9,** 1–14 (2014).

11. Gil, F. N., Moreira-Santos, M., Chelinho, S., Pereira, C., Feliciano, J. R., Leitão, J. H.,

Sousa, J. P., Ribeiro, R., Viegas, C. A. Suitability of a Saccharomyces cerevisiae -based assay to assess the toxicity of pyrimethanil sprayed soils via surface runoff : Comparison with standard aquatic and soil toxicity assays. *Sci. Total Environ.* **505,** 161–171 (2015).

12. Fernandes, A. R. & Sá-Correia, I. The activity of plasma membrane H+-ATPase is strongly stimulated during Saccharomyces cerevisiae adaptation to growth under high copper stress, accompanying intracellular acidification. *Yeast* **18,** 511–512 (2001).

13. Gerstein, A. C., Lo, D. S., Campbell, M. L., Kuzmin, A. & Otto, S. P. in *Genetics: Early Online* (2014).

14. Avery, S. V, Howlett, N. G. & Radice, S. Copper toxicity towards Saccharomyces cerevisiae: dependence on plasma membrane fatty acid composition. *Appl. Environ. Microbiol.* **62,** 3960–3966 (1996).

15. Chen, X., Udalagama, C. N.B., Chen, C., Bettiol, A. A., Pickard, D. S., Venkatesan, T., Watt, F. Whole-Cell Imaging at Nanometer Resolutions Using Fast and Slow Focused Helium Ions. *Biophys. J.* **101,** 1788–1793 (2011).

16. Watt, F., Rajendran, R., Ren, M. Q., Tan, B. K. H. & Halliwell, B. A nuclear microscopy study of trace elements Ca, Fe, Zn and Cu in atherosclerosis. *Nucl. Instruments Methods Phys. Res. Sect. B Beam Interact. with Mater. Atoms* **249,** 646–652 (2006).

17. Pinheiro, T., Ynsa, M. D. & Alves, L. C. Imaging biological structures with a proton microprobe *Modern Research and Educational Topics in Microscopy* 237–244 (2007).

18. Cho, W.-S. *et al.* Predictive value of in vitro assays depends on the mechanism of toxicity of metal oxide nanoparticles. *Part. Fibre Toxicol.* **10,** 55 (2013).

19. Pokhrel, S., Nel, E. E. & Madler, L. Custom-Designed Nanomaterial Libraries for Testing Metal Oxide Toxicity. *Acc. Chem. Res.* **46,** 632–641 (2012).

20. Bloomber BNA. Proposal for CPSC Nanotechnology Center Would Study Consumer Health Risks BY. *Prod. Saf. Liabil. Reporter™* **43,** (2015).

21. http://ec.europa.eu/research/industrial_technologies/nanoscience-and-technologies_en.html (Consulted at 2015-11-25).

22. Ren, G., Hu, D., Cheng, E. W. C., Vargas-Reus, M. A., Reip, P., Allaker, R. P. Characterisation of copper oxide nanoparticles for antimicrobial applications. *Int. J. Antimicrob. Agents* **33,** 587–590 (2009).

23. Bour, A., Mouchet, F., Silvestre, J., Gauthier, L. & Pinelli, E. Environmentally relevant approaches to assess nanoparticles ecotoxicity: A review. *J. Hazard. Mater.* **283,** 764–

777 (2015).

24. Giannousi, K., Sara, G., Mourdikoudis, S. & Pantazaki, A. Selective Synthesis of Cu 2 O and Cu/Cu 2 O NPs : Antifungal Activity to Yeast Saccharomyces cerevisiae and DNA Interaction. *Inorg. Chem.* **53,** 9657−9666 (2014).

25. Athanassiou, E. K., Grass, R. N. & Stark, W. J. Large-scale production of carbon-coated copper nanoparticles for sensor applications. *Nanotechnology* **17,** 1668–1673 (2006).

26. Ruparelia, J. P., Chatterjee, A. K., Duttagupta, S. P. & Mukherji, S. Strain specificity in antimicrobial activity of silver and copper nanoparticles. *Acta Biomater.* **4,** 707–716 (2008).

27. Morones, J. R., Elechiguerra, J. L., Camacho, A., Holt, K., Kouri, J. B., Ramírez, J. T., Yacaman, M. J. The bactericidal effect of silver nanoparticles. *Nanotechnology* **16,** 2346–2353 (2005).

28. Magdassi, S., Grouchko, M. & Kamyshny, A. Copper Nanoparticles for Printed Electronics: Routes Towards Achieving Oxidation Stability. *Materials (Basel).* **3,** 4626–4638 (2010).

29. Lee, Y., Choi, J., Lee, K. J., Stott, N. E. & Kim, D. Large-scale synthesis of copper nanoparticles by chemically controlled reduction for applications of inkjet-printed electronics. *Nanotechnology* **19,** 415604 (2008).

30. Kwak, K. & Kim, C. Viscosity and thermal conductivity of copper oxide nanofluid dispersed in ethylene glycol. *Korea Aust. Rheol. J.* **17,** 35–40 (2005).

31. Treuel, L., Jiang, X. & Nienhaus, G. U. New views on cellular uptake and trafficking of manufactured nanoparticles New views on cellular uptake and trafficking of manufactured nanoparticles. *J. R. Soc.* (2013).

32. Santos, S. C. dos, Teixeira, M. C., Cabrito, T. R. & Sá-Correia, I. Yeast toxicogenomics: genome-wide responses to chemical stresses with impact in environmental health, pharmacology, and biotechnology. *Front. Genet.* **3,** 1–17 (2012).

33. Dos Santos, S. C. & Sá-Correia, I. Yeast toxicogenomics: lessons from a eukaryotic cell model and cell factory. *Curr. Opin. Biotechnol.* **33,** 183–191 (2015).

34. Howlett, N. G. & Avery, S. V. Induction of Lipid Peroxidation during Heavy Metal Stress in Saccharomyces cerevisiae and Influence of Plasma Membrane Fatty Acid Unsaturation. **63,** 2971–2976 (1997).

35. Herdeiro, R. S. & Pereira, M. D. Trehalose protects Saccharomyces cerevisiae from lipid peroxidation during oxidative stress Keywords. *Biochim. Biophys. Acta* **1760,** 340–346 (2006).

36. Azevedo, F., Marques, F., Fokt, H., Oliveira, R. & Johansson, B. Measuring oxidative DNA damage and DNA repair. *Yeast* 55–61 (2011). doi:10.1002/yea

37. Poli, P. *et al.* Comet assay application in environmental monitoring : DNA damage in human leukocytes and plant cells in comparison with bacterial and yeast tests. **14,** 547–555 (1999).

38. Guecheva, T., Henriques, J. A. P. & Erdtmann, B. Genotoxic effects of copper sulphate in freshwater planarian in vivo , studied with the single-cell gel test (comet assay) Keywords. **497,** 15–19 (2001).

39. Costa, V., Quintanilha, A. & Moradas-Ferreira, P. Protein oxidation, repair mechanisms and proteolysis in Saccharomyces cerevisiae. *IUBMB Life* **59,** 293–298 (2007).

40. Dias, P. J. & Teixeira, M. C. Insights into the Mechanisms of Toxicity and Tolerance to the Agricultural Fungicide Mancozeb in Yeast , as Suggested by a Chemogenomic Approach. **14,** (2010).

41. Kim, J., Yoon, H. W. & Kwon, K. Identification of Proteins Containing Cysteine Residues That Are Sensitive to Oxidation by Hydrogen Peroxide at Neutral pH Keywords. **283,** 2000–2002 (2000).

42. Thiele, D. J. ACE1 regulates expression of the Saccharomyces cerevisiae metallothionein gene. *Mol. Cell. Biol.* **8,** 2745–52 (1988).

43. Culottal, V. C., Howards, W. R. & Liu, X. F. CRS5 Encodes a Metallothionein-like Protein in Saccharomyces cerevisiae. *J. Biol. Chem.* **269,** 25295–25302 (1994).

44. Lazo, J. S., Kuo, S. M., Woo, E. S. & Pitt, B. R. The protein thiol metallothionein as an antioxidant and protectant against antineoplastic drugs. *Chem Biol Interact* **111-112,** 255–262 (1998).

45. Viarengo, A., Burlando, B., Ceratto, N. & Panfoli, I. Antioxidant role of metallothioneins: a comparative overview. *Cellular and Molecular Biology* **46,** 407–417 (2000).

46. Ruttkay-Nedecky, B. *et al.* The role of metallothionein in oxidative stress. *Int. J. Mol. Sci.* **14,** 6044–6066 (2013).

47. Festa, R. A. & Thiele, D. J. Copper: An essential metal in biology. *Curr. Biol.* **21,** R877–R883 (2011).

48. Nevitt, T., Öhrvik, H. & Thiele, D. J. Charting the travels of copper in eukaryotes from yeast to mammals. *Biochim. Biophys. Acta - Mol. Cell Res.* **1823,** 1580–1593 (2012).

49. Foster, A. W. *et al.* A chemical potentiator of copper-accumulation used to investigate the iron-regulons of Saccharomyces cerevisiae. *Mol. Microbiol.* **93,** 317–330 (2014).

50. Cascio, C., Gilliland, D., Rossi, F., Calzolai, L. & Contado, C. Critical Experimental Evaluation of Key Methods to Detect, Size and Quantify Nanoparticulate Silver. *Anal. Chem.* **86,** 12143−12151 (2014).

51. NanoComposix. Guide to Dynamic Light Scattering Measurement and Analysis. **v 1.3,** (2012).

52. Hassan, P. a, Rana, S. & Verma, G. Making Sense of Brownian Motion: Colloid Characterization by Dynamic Light Scattering. *Langmuir* (2014). doi:10.1021/la501789z

53. Merdzan, V., Domingos, R. F., Monteiro, C. E., Hadioui, M. & Wilkinson, K. J. The effects of different coatings on zinc oxide nanoparticles and their influence on dissolution and bioaccumulation by the green alga, C. reinhardtii. *Sci. Total Environ.* **488-489,** 316–324 (2014).

54. Everett, W. N., Chern, C., Sun, D., Mcmahon, R. E., Zhang, X., Chen, W. A., Hahn, M. S., Sue, H. Phosphate-enhanced cytotoxicity of zinc oxide nanoparticles and agglomerates. *Toxicol. Lett.* **225,** 177–184 (2014).

55. Gontier, E., Ynsa, M., Bíró, T., Hunyadi, J., Kiss, B., Gáspár, K., Pinheiro, T., Silva, J., Filipe, P., Stachura, J., Dabros, W., Reinert, T., Butz, T., Moretto, P., Surlève-Bazeille, J. Is there penetration of titania nanoparticles in sunscreens through skin? A comparative electron and ion microscopy study. *Nanotoxicology* **2,** 218–231 (2008).

56. Pinheiro, T., Pallon, J., Alves, L.C., Veríssimo, A., Filipe, P., Silva, J.N., Silva, R. The influence of corneocyte structure on the interpretation of permeation profiles of nanoparticles across skin. *Nucl. Instruments Methods Phys. Res. Sect. B Beam Interact. with Mater. Atoms* **260,** 119–123 (2007).

57. Godinho, R. M., Cabrita, T., Alves, C. & Pinheiro, T. Imaging of intracellular metal partitioning in marine diatoms exposed to metal pollution : consequences to cellular toxicity and metal fate in the environment. *Metallomics* (2014). doi:10.1039/c4mt00105b

58. Chen, X., Chen, C., Udalagama, C. N. B., Ren, M., Fong, K. E., Yung, L. Y. L., Giorgia, P., Bettiol, A. A., Watt, F. High-resolution 3D imaging and quantification of gold nanoparticles in a whole cell using scanning transmission ion microscopy. *Biophys. J.* **104,** 1419–25 (2013).

59. Grime, G. W. & Dawson, M. Recent developments in data acquisition and processing on the Oxford scanning proton microprobe. *Nucl. Instruments Methods Phys. Res. Sect. B*

Beam Interact. with Mater. Atoms **104,** 107–113 (1995).

60. Grime, G. W. The ‘ Q factor’ method: quantitative microPIXE analysis using RBS normalisation. *Nucl. Instruments Methods Phys. Res. Sect. B Beam Interact. with Mater. Atoms* **109-110,** 170–174 (1996).

61. Klis, F. M., Mol, P., Hellingwerf, K. & Brul, S. Dynamics of cell wall structure in Saccharomyces cerevisiae. *FEMS Microbiol.Rev.* **26,** 239–256 (2002).

62. Dönmez, G. & Aksu, Z. The effect of copper(II) ions on the growth and bioaccumulation properties of some yeasts. *Process Biochem.* **35,** 135–142 (1999).

63. Avery, S. V, Howlett, N. G. & Radice, S. Copper toxicity towards Saccharomyces cerevisiae: dependence on plasma membrane fatty acid composition. *Appl. Environ. Microbiol.* **62,** 3960–3966 (1996).

64. Jamieson, D. J. Oxidative stress responses of the yeast Saccharomyces cerevisiae. *Yeast* **14,** 1511–1527 (1998).

65. Peña, M. M., Koch, K. a & Thiele, D. J. Dynamic regulation of copper uptake and detoxification genes in Saccharomyces cerevisiae. *Mol. Cell. Biol.* **18,** 2514–2523 (1998).

66. Bayat, N., Rajapakse, K., Marinsek-Logar, R., Drobne, D. & Cristobal, S. The effects of engineered nanoparticles on the cellular structure and growth of Saccharomyces cerevisiae. *Nanotoxicology* **8,** 363–73 (2014).

67. Ohnuki, T., Sakamoto, F., Kozai, N., Ozaki, T., Narumi, I., Francis, A. J., Iefuji, H., Sakai, T., Kamiya, T., Satoh, T., Oikawa, M. Application of micro-PIXE technique to uptake study of cesium by Saccharomyces cerevisiae. *Nucl. Instruments Methods Phys. Res. Sect. B Beam Interact. with Mater. Atoms* **210,** 378–382 (2003).

68. Kern, A. L., Bonatto, D., Dias, J. F., Yoneama, M., Brendel, M. Pêgas Henriques, J. A. The function of Alr1p of Saccharomyces cerevisiae in cadmium detoxification: insights from phylogenetic studies and particle-induced X-ray emission. *Biometals an Int. J. role Met. ions Biol. Biochem. Med.* **18,** 31–41 (2005).

69. Ortega, R. Micro-Pixe for Single Cell Analysis. *Int. J. PIXE* **22,** 51–56 (2012).

70. Watt, F., Grime, G. W., Brook, A. J., Gadd, G. M., Perry, C. C., Pearce, R. B., Turnau, K., Watkinson, S. C. Nuclear microscopy of biological specimens. *Nucl. Instruments Methods Phys. Res. Sect. B Beam Interact. with Mater. Atoms* **54,** 123–143 (1991).

71. Cronholm, P., Karlsson, H. L., Hedber, J., Lowe, T. A., Winnberg, L., Elihn, K., Wallinder, I. O., Moller, L. The effects of brief mindfulness intervention on acute pain experience: An

examination of individual difference. *Small* **7,** 970–982 (2013).

72. Tenzer, S., Docter, D., Kuharev, J., Musyanovych, A., Fetz, V., Hecht, R., Schlenk, F., Fischer, D., Kiouptsi, K., Reinhardt, C., Landfester, K., Schild, H., Maskos, M., Knauer, S. K., Stauber, R. H. Rapid formation of plasma protein corona critically affects nanoparticle pathophysiology. *Nat. Nanotechnol.* **8,** 772–81 (2013).

Annexes

8 Annex I

8.1 CuO-NPs characterization

8.1.1 Optimization of the methodology and contamination control

Different concentrations of CuO-NPs were tested in aqueous and MM4 medium, different equilibration times and data acquisition times, in order to optimize the analytical protocol. The nanoparticles average size distribution was initially studied in an aqueous medium, taking into account the temporal parameters: equilibration and analysis time. It was found that equilibration times (t_{eq}) inferior than 120s were insufficient to guarantee the stability of the suspension and the quality of the analysis also improved for acquisition times ($t_{analysis}$) smaller than 60s per measure (run). Short equilibration times (up to 60 s) and analysis times (up to 60s) did not allow reliable results, as can be seen in Table 8.1 by the inconsistent values Z-average and Intensity Mean and by the very high PdI values (> 0.5), indicating very broad and not monomodal distributions.

Table 8.1 DLS analysis of CuO-NPs in aqueous suspension.
The average hydrodynamic diameter of particles calculated by the Z-Average Intensity Mean and methods; PdI polydispersion index. The PDI values represent the dispersion of sizes present in the sample

CuO-NPs (mgCu/L)	t_{eq} (s)	$t_{analysis}$ (s)	Z-Average (d.nm)	PdI	Intensity Mean (d.nm)
3	5	5	13551.00 ± 6824.07	0.92 ± 0.12	0.00 ± 0.00
	10	5	13590.83 ± 14300.54	0.82 ± 0.26	64.12 ± 55.88
25	20	15	845.48 ± 425.83	0.66 ± 0.32	287.30 ± 134.34
		60	491.08 ± 244.93	0.39 ± 0.18	351.25 ± 157.77
	60	60	460.30 ± 39.39	0.44 ± 0.02	408.08 ± 16.84
		90	928.12 ± 873.70	0.58 ± 0.22	355.32 ± 92.46
30	5	5	1905.00 ± 468.91	0.91 ± 0.09	366.07 ± 100.96
		10	1851.67 ± 193.25	0.89 ± 0.08	413.42 ± 63.26
		15	1695.33 ± 196.17	0.87 ± 0.08	390.82 ± 111.20
	10	10	1585.45 ± 810.37	0.77 ± 0.24	415.48 ± 113.48
	20	15	1055.95 ± 476.92	0.55 ± 0.16	558.20 ± 73.89
300	10	11	1729.67 ± 45.83	0.40 ± 0.03	1232.33 ± 50.74

The behaviour of NPs in the biological medium was studied, taking into account the results obtained in preliminaries tests. Samples of CuO-NPs suspensions in MM4 media with 10 and 20 mgCu/L of CuO-NPs were analysed in MM4 growth medium (Table 8.2). The results were only satisfactory, taking into account the PdI values. However the average diameter of the nanoparticles increased, which suggests modification of the particle surface when in MM4 medium. Therefore differences were observed between the Z-Average and Intensity Mean values, regardless of the concentration of nanoparticles in the biological environment, reflecting the presence of populations with different particle diameters of the NPs in the suspension.

Table 8.2 CuO-NPs suspensions analysis in MM4 in liquid medium.
Average hydrodynamic diameter of particles calculated by the Z-Average and Intensity Mean methods; PdI polydispersion index. The **Pd**I values represent the dispersion of sizes present in the sample. The particle size and its distribution indicators are displayed in 3 successive measurements of the same sample after 1, 26 and 50 h of the suspension preparation.

CuO-NPs (mgCu/L)	Time (h)	Z-Average (d.nm)	PdI	Intensity Mean (d.nm)
10	1	1381.67 ± 25.58	0.496 ± 0.077	849.10 ± 75.29
	26	1500.50 ± 252.54	0.646 ± 0.054	729.60 ± 69.55
	50	2556.75 ± 1728.12	0.777 ± 0.258	778.53 ± 315.49
20	1	1311.00 ± 194.58	0.475 ± 0.245	887.00 ± 242.55
	26	1901.20 ± 314.46	0.663 ± 0.192	834.10 ± 181.93
	50	2341.25 ± 728.94	0.508 ± 0.341	1138.40 ± 572.83

8.1.2 Contamination control

Initial tests showed that some samples had very clear deviations, taking into account the results for the same sample replicates, prepared at different times. The results obtained considering multiple parameters provided by the software (value of the correlation function, chi-square function setting, PdI, among others) showed that the sample contained contaminations that could have originated in the laboratory material (disposable glass) used. As an example, shown in Table 8.2, are the data obtained for trials with CuO-NPs dispersed in MM4, with concentrations of 10 and 20 mgCu/L, in glass containers, used in biological assays. Successive measurements of the same sample were made during 48 h. All samples were shaken vigorously before testing. The high values of PdI (~ 0.5 or higher) and large discrepancy between the Z-Average and Intensity Mean values. The ratio Mean Intensity / Z-Average were lower than 0.61 indicating a diameters dispersion of the nanoparticles, with the occasional presence of large particles. This may be due to the presence of impurities in the samples. Tests on standard polystyrene beads with a 0,69µm diameter, using glass material, also originated random fluctuations of the results. In 18 successive tests there were anomalies in the PdI values (greater than 0.8) and discrepancies between the values of Z-Average and Intensity Mean, contrasting with the results shown in Table 4.1, when rigorous control of reagents and analytical procedures was ensured.

8.1.3 CuO-NPs dimensions in MM4 liquid medium

Table 8.3 CuO-NPs suspensions analysis in MM4 in liquid medium, throughout the exposure tests. The particle size and its distribution indicators are displayed (PdI, and Z-Average Intensity Mean) in successive measurements of the same sample for 48 h, after the suspension preparation.

CuO-NPs (mgCu/L)	Time	Z-Average (d,nm)	PdI	Intensity Mean (d,nm)
10	0	1141.50 ± 71.42	0.658 ± 0.001	501.30 ± 2.26
	2	1111.00 ± 11.32	0.565 ± 0.001	612.60 ± 2.97
	4	1104.50 ± 24.75	0.532 ± 0.013	676.20 ± 14.57
	6	1110.50 ± 12.02	0.497 ± 0.043	703.15 ± 68.66
	8	1198.00 ± 1.41	0.442 ± 0.059	845.25 ± 2.62
	24	1691.67 ± 147.06	0.777 ± 0.154	556.97 ± 199.32
	31	1807.50 ± 211.42	0.820 ± 0.100	592.15 ± 171.05
	48	1836.00 ± 514.77	0.589 ± 0.165	1879.50 ± 570.64
15	0	1026.00 ± 25.46	0.414 ± 0.025	754.90 ± 13.15
	2	1048.50 ±2.12	0.432 ± 0.019	734.85 ± 8.27
	4	1046.00 ± 69.30	0.399 ± 0.088	737.90 ± 102.95
	6	978.20 ± 13.39	0.411 ± 0.105	709.75 ± 54.52
	8	1052.00 ± 5.66	0.489 ± 0.035	683.45 ± 36.13
	24	1055.50 ± 21.92	0.565 ± 0.012	591.70 ± 18.24
	31	1434.00 ± 316.78	0.640 ± 0.154	700.50 ± 17.82
	48	1434.00 ± 49.50	0.601 ± 0.138	722.85 ± 154.64
20	0	1070.50 ± 19.09	0.411 ± 0.037	765.65 ± 24.68
	2	1042.50 ± 4.95	0.374 ± 0.023	800.85 ± 7.85
	4	1086.50 ± 3.54	0.294 ± 0.099	859.35 ± 57.91
	6	1128.00 ± 67.88	0.461 ± 0.132	786.60 ± 138.73
	8	1213.00 ± 60.81	0.363 ± 0.084	866.20 ± 59.11
	24	1185.00 ± 2.83	0.519 ± 0.031	705.80 ± 33.09
	31	1262.00 ± 25.46	0.406 ± 0.021	907.15 ± 35.14
	48	1395.00 ± 5.66	0.645 ± 0.103	665.55 ± 100.34
40	0	1096.50 ± 33.23	0.334 ± 0.011	922.05 ± 64.56
	2	1293.00 ± 55.15	0.290 ± 0.015	1304.50 ± 286.38
	4	1128.00 ± 19.80	0.461 ± 0.037	786.60 ± 185.19

CuO-NPs (mgCu/L)	Time	Z-Average (d,nm)	PdI	Intensity Mean (d,nm)
40	6	1333.00 ± 74.95	0.316 ± 0.008	1329.00 ± 65.05
	8	1285.50 ± 21.92	0.304 ± 0.040	1264.50 ± 163.34
	24	1107.00 ± 35.36	0.266 ± 0.077	963.35 ± 31.47
	31	1408.50 ± 16.26	0.272 ± 0.042	1264.50 ± 154.86
	48	1649.00 ± 104.65	0.333± 0.081	1318.50 ± 106.77

9 Annex II

9.1 Elemental concentrations in *S. cerevisiae* strains, after Cu exposure

The elemental concentrations determined in *S. cerevisiae* strains are plotted in the following graphs. Results plotted were summarized as average and standard deviations based on the number of point analysis (cells) performed for each experimental condition (N > 5). The exploratory analysis to assess differences between exposure conditions, growth phase and strain was also evaluated, although the discussion of results was restricted to Cu. Therefore, all the significant results are identified in the graphs, although no further appreciation concerning the physiological significance of these changes for elements other than Cu were presented in this thesis.

Figure 9.1 show the elemental concentrations measured in wild-type strain for the different exposure concentrations of $CuSO_4$. Figure 9.2 show the elemental concentrations measured in wild-type strain for the different exposure concentrations of CuO-NPs. Both tests were analysed at two incubation stages, i.e., 6h and 24h.

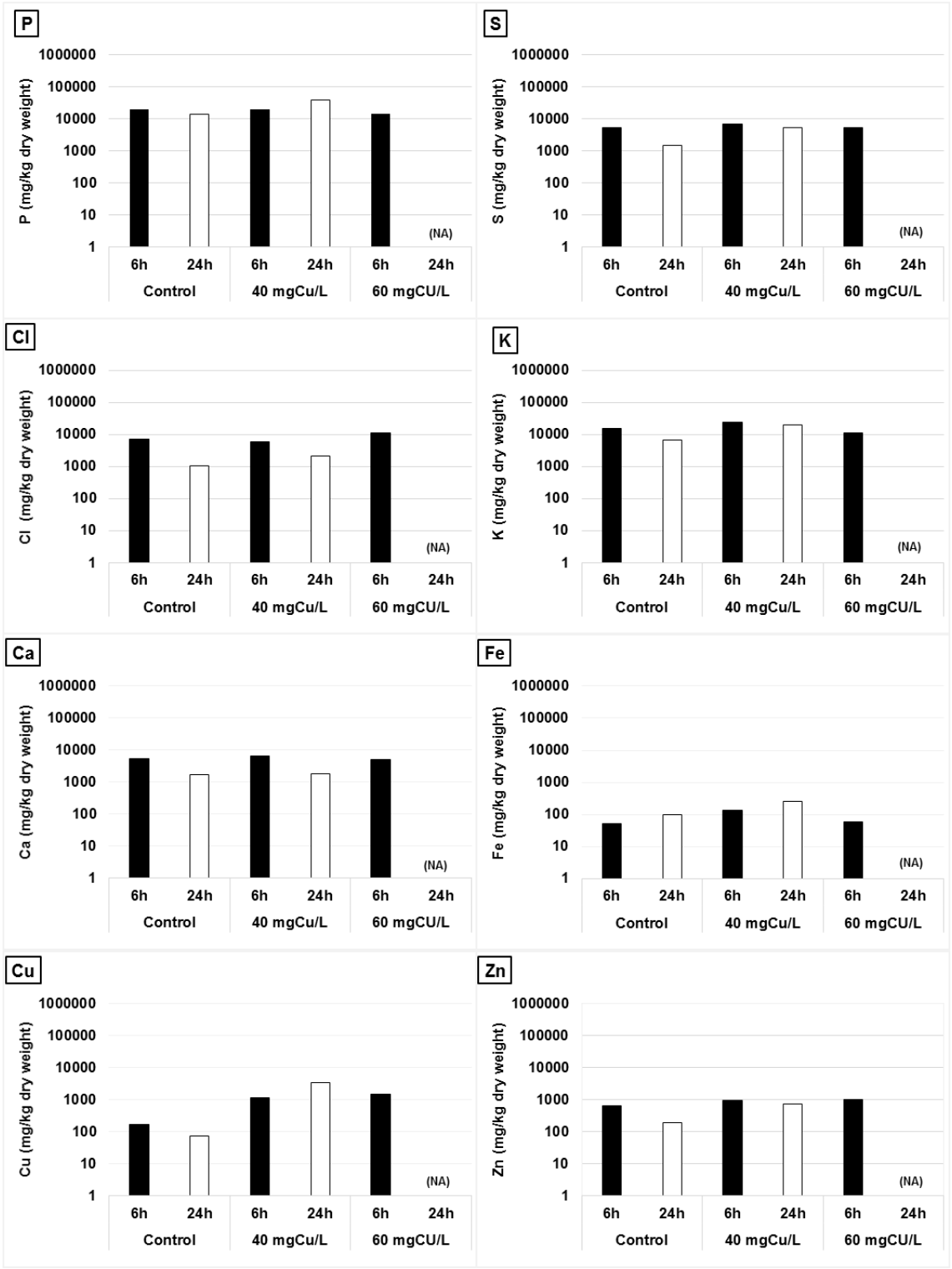

Figure 9.1 Elemental concentrations in *Saccharomyces cerevisiae* BY4741 cells growing in MM4 liquid medium in the presence of $CuSO_4$.
The *S. cerevisiae* BY4741 cells were collected after 6h of growth (black) and after 24h (white) in the presence of 40 mgCu/ L and 60 mgCu/L of $CuSO_4$. Cells not supplemented with $CuSO_4$ served as controls (Control)**.** Some conditions were not analysed (NA).

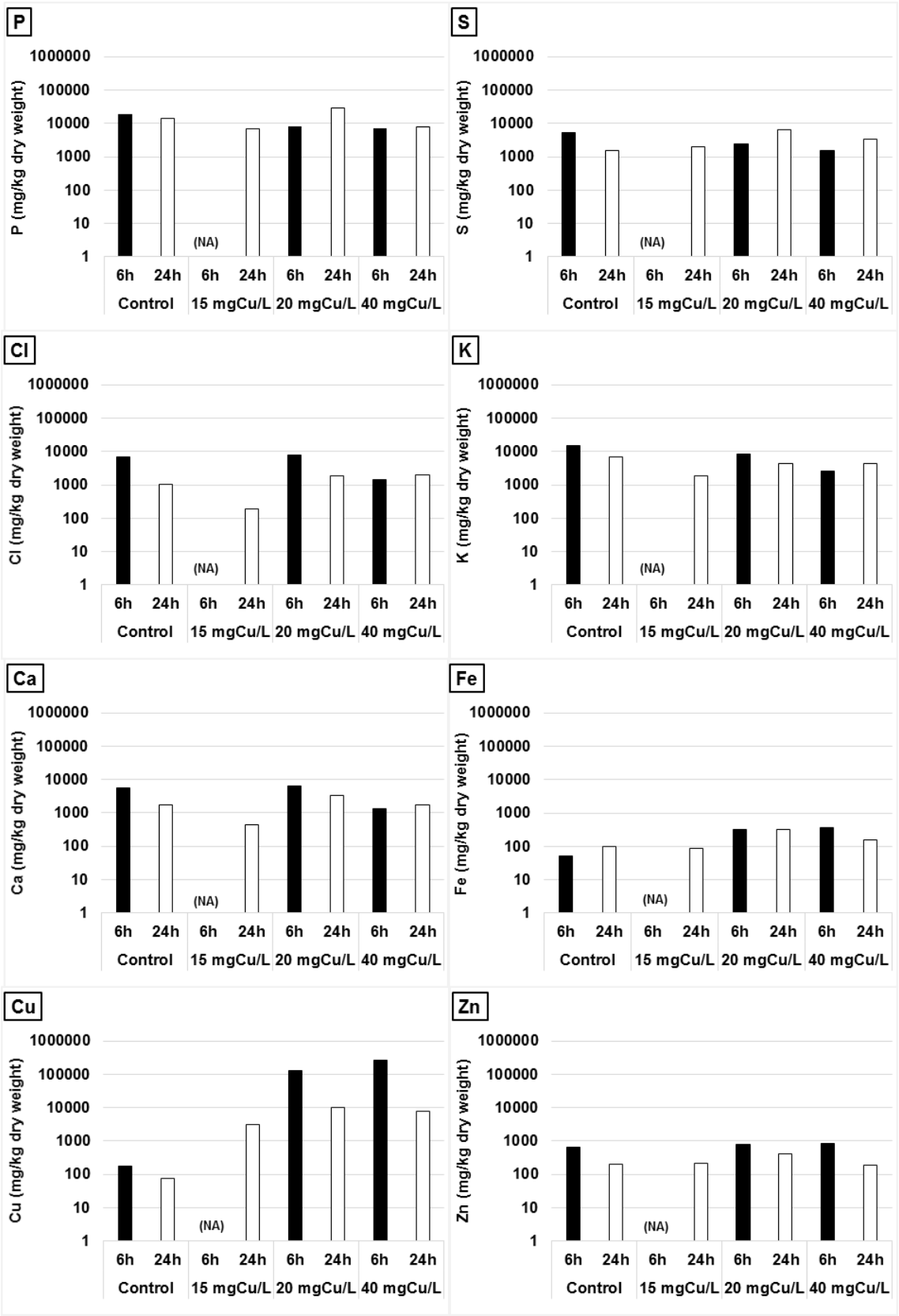

Figure 9.2 Elemental concentrations in *Saccharomyces cerevisiae* BY4741 cells growing in MM4 liquid medium in the presence of CuO-NPs.
The *S. cerevisiae* BY4741 cells were collected after 6h of growth (dark grey) and after 24h (light grey) in the presence of 15 mgCu/L, 20 mgCu/L and 40 mgCu/L of CuO-NPs. Cells not supplemented with CuO-NPs nor $CuSO_4$ served as controls (Control). Some conditions were not analysed (NA).

Figure 9.3 show the elemental concentrations measured in Δ*cup2* cells, after 6h of incubation with CuO-NPs and $CuSO_4$. Three levels of exposure are plotted, i.e., 6 mgCu/L, 10 mgCu/L and 40 mgCu/L.

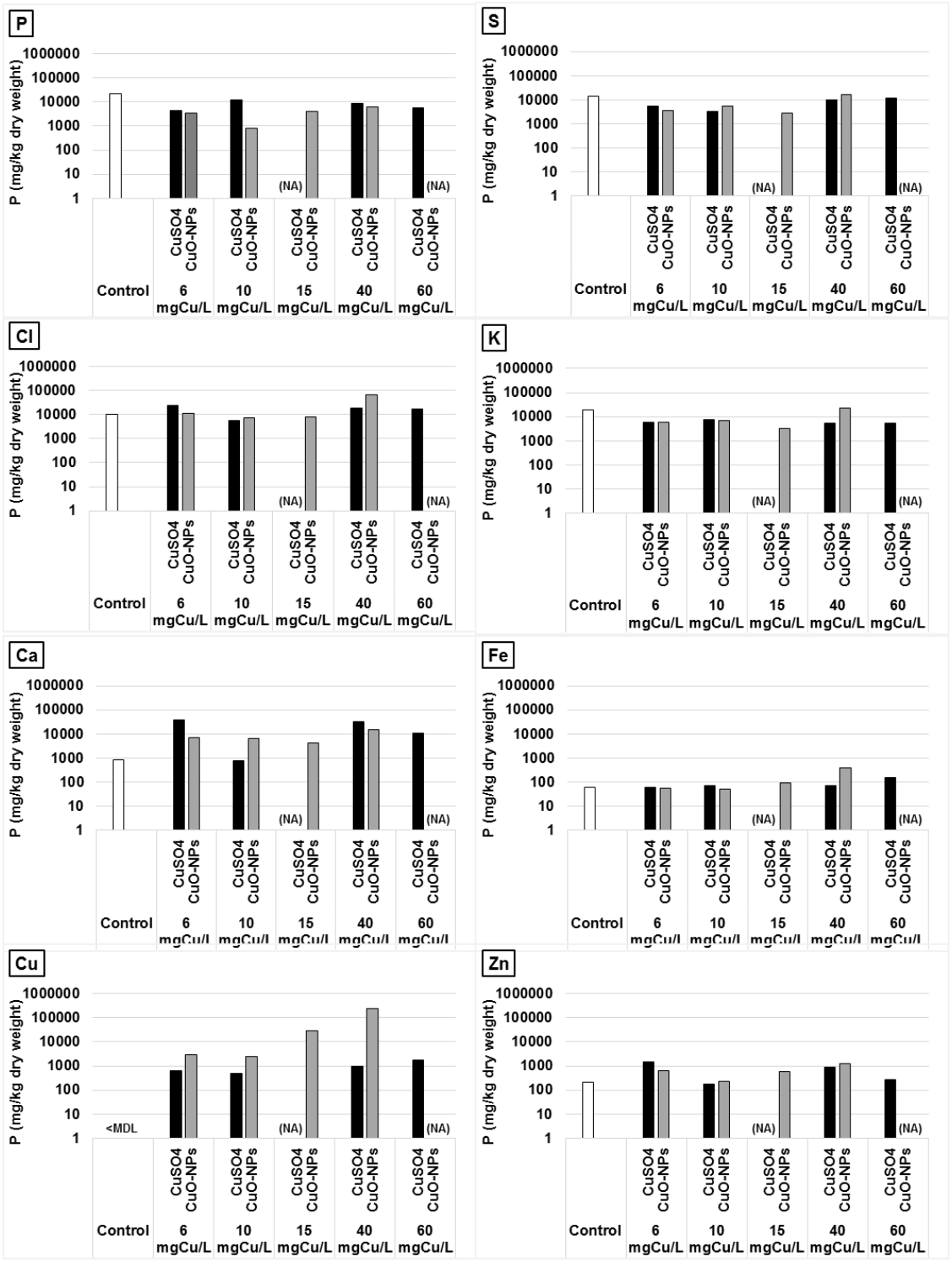

Figure 9.3 Average elemental concentrations and relative standard deviations in *Saccharomyces cerevisiae* BY4741_ *Δcup2* cells growing in MM4 liquid medium in the presence of $CuSO_4$ and CuO-NPs.

The *S. cerevisiae* BY4741 cells were collected after 6h of growth in the presence of 6mgCu/L, 10mgCu/L and 40mgCu/L of $CuSO_4$ or 6mgCu/L, 10mgCu/L and 40mgCu/L of CuO-NPs. As control it were used cells not supplemented with CuO-NPs nor $CuSO_4$. Values under the minimal detection limit are represented with <MDL. Some conditions were not analysed (NA).